Available online at www.sciencedirect.com
ScienceDirect
Journal of Asian Earth Sciences 33 (2008) 61–77
Journal of Asian Earth Sciences
www.elsevier.com/locate/jaes

Geochemistry of Paleoproterozoic (~1770 Ma) mafic dikes from the Trans-North China Orogen and tectonic implications

Yuejun Wang [a,d,*], Guochun Zhao [b], Peter A. Cawood [c], Weiming Fan [a], Touping Peng [a], Linhua Sun [a]

[a] Key Laboratory of Isotope Geochronology and Geochemistry, Guangzhou Institute of Geochemistry, Chinese Academy of Sciences, P.O. Box 1131, Guangzhou 510640, People's Republic of China
[b] Department of Earth Sciences, The University of Hong Kong, Pokfulam Road, Hong Kong
[c] Tectonics Special Research Centre, The University of Western Australia, Crawley, WA 6009, Australia
[d] Department of Earth Sciences, Northwest University, Xi'an 710069, China

Received 14 July 2007; received in revised form 5 October 2007; accepted 23 October 2007

Abstract

Paleoproterozoic (~1770 Ma) mafic dikes occur throughout the Trans-North China Orogen. These dikes can be divided into three geochemically distinct groups. Group 1 with FeOt of 12.73–18.06%, $(Nb/La)_N$ 0.18–0.39, $(Th/La)_N$ of, 0.60–1.24, $\varepsilon_{Nd}(t)$ of −5.1 to −2.4, and an enrichment in LILE's and a depletion in HFSE's. Group 2 has flat REEs and incompatible elements patterns, and possesses $(Nb/La)_N = 0.64–0.87$, $(Th/La)_N = 0.61–1.20$ and $\varepsilon_{Nd}(t) = -1.7$ to 1.1. Group 3 has low FeOt contents (8.19–11.57%) and $(Th/La)_N$ ratios (0.29–0.72), but similar $(Nb/La)_N$ ratios and $\varepsilon_{Nd}(t)$ values to those of Group 1. Petrological and geochemical data suggest that these dikes may have originated from different sources. Group 1 could be derived from a "re-fertilized" lithospheric source incorporating a continental basaltic component trapped from a earlier phase of subduction. Group 2 was likely a product of a subduction-modified lithospheric mantle hybridized by recycled gabbroic lower crust. By contrast, Group 3 originated from a mixture of subduction-modified lithospheric mantle with a MORB component. In combination with the available data, we propose that the sources of the mafic dikes were initially modified by the ~1.85 Ga subduction/collision event that assembled the North China Craton, and partially melted under subsequent rifting in response to the upwelling convective mantle.

Keywords: Geochemistry; Mafic dikes; Subduction-related lithospheric mantle; Paleoproterozoic; Trans-North China Orogen

1. Introduction

In the last decade, numerous structural, lithological, metamorphic, geochemical and geochronological investigations have been carried out to probe into the Precambrian evolution of the North China Craton (e.g. Cawood et al., 1998; Kröner et al., 2005, 2006; Zhao et al., 2000, 2003, 2005; Zhai and Liu, 2003; Wang et al., 2003, 2004). It is generally agreed that the North China Craton is composed of two different blocks that developed independently and finally collided to form a coherent craton (Fig. 1a) (e.g. Zhao et al., 2005 and references therein). However, timing of the final amalgamation of the North China Craton is still debated. Li et al. (2000) and Kusky and Li (2003) argued that the two Achaean blocks of the North China Craton (the Eastern and Western Blocks) were amalgamated by a ~2.5 Ga collisional event, and that the ~1.85 Ga Lüliang event (traditionally named the "Lüliang Movement") represents an intra-continental rifting event in the craton, whereas others favor the

* Corresponding author. Present address: Key Laboratory of Isotope Geochronology and Geochemistry, Guangzhou Institute of Geochemistry, Chinese Academy of Sciences, P.O. Box 1131, Guangzhou 510640, People's Republic of China. Tel.: +86 20 85290527; fax: +86 20 85291510.
E-mail address: yjwang@gig.ac.cn (Y. Wang).

1367-9120/$ - see front matter © 2007 Elsevier Ltd. All rights reserved.
doi:10.1016/j.jseaes.2007.10.018

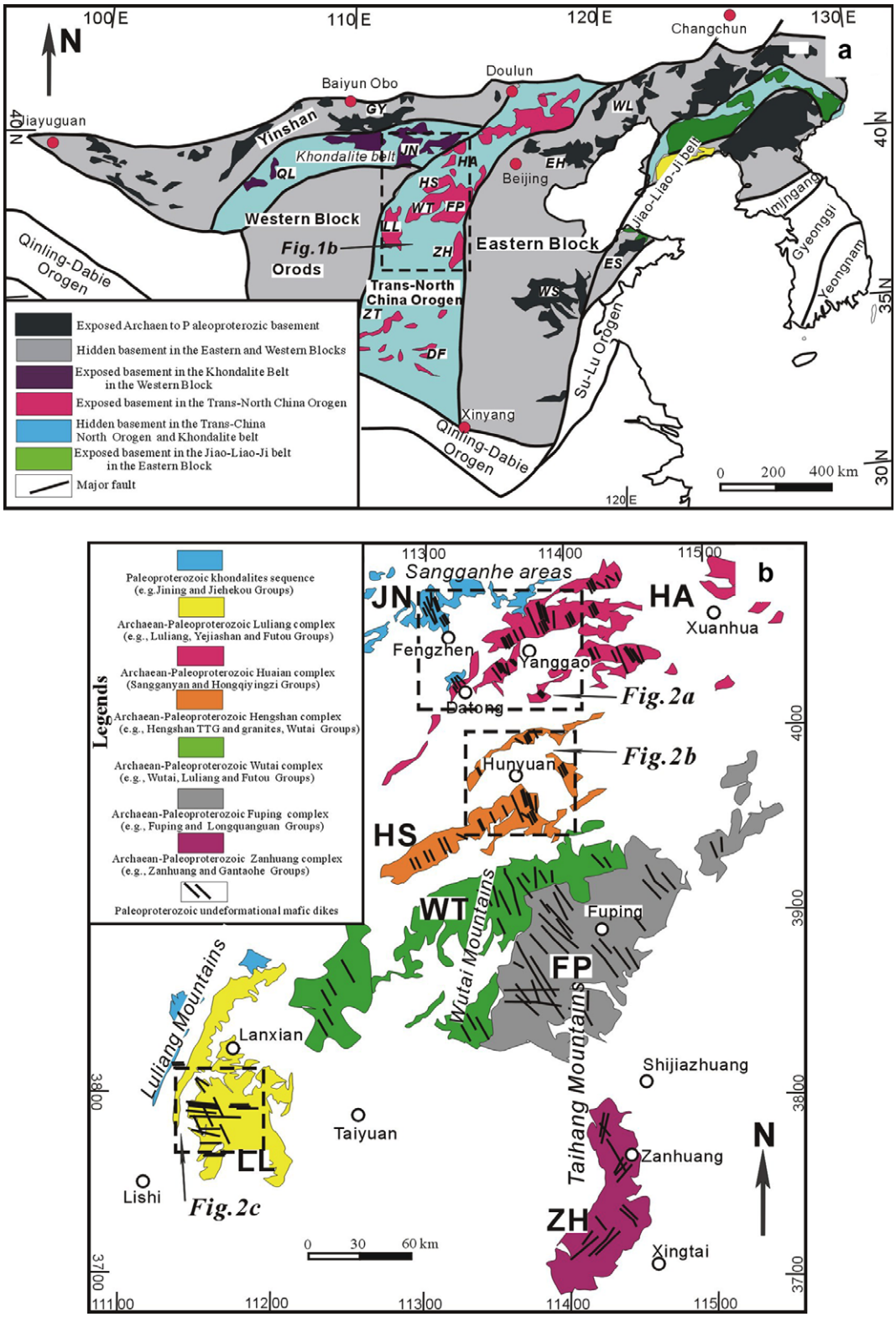

Fig. 1. (a) Schematic map showing tectonic subdivision of the North China Craton (after Zhao et al., 2005), with locations of the Zhongtiao (ZT), Dengfeng (DF), Guyang (GY), Lüliang (LL), Jining (JN), Huai'an (HA), Western Liaoning (WL), Eastern Hebei (EH), Western Shandong (WS), Hengshan (HS), Wutai (WT), Lüliang (LL), Fuping (FP) and Zanhuang (ZH) domains. (b) Geological map showing the distribution of the Paleoproterozoic mafic dikes in the Trans-North China Orogen (revised after HBBGMR, 1989; SXBGMR, 1989; IMBGMR, 1991).

model that the two blocks subducted and subsequently collided along the Trans-North China Orogen at ~1.85 Ga (e.g. Zhao et al., 2000, 2003, 2005; Kröner et al., 2005, 2006).

Recent data show that this Paleoproterozoic tectonic event was followed by an extensional event, marked by the occurrence of mafic swarms at 1781–1765 Ma (Halls et al., 2000; Wang et al., 2004; Peng, 2005). However, controversy has surrounded the tectonic setting of these mafic dike swarms. One school of thought argues that these swarms are related to a mantle plume event that led to the break-up of the North China Craton from other cratons (e.g. Peng, 2005); whereas others believe that these dikes were generated in a post-collisional extension setting (e.g. Wang et al., 2003, 2004). Geochemical character of these dikes needs to be established to resolve this issue and initial geochemical and geochronological investigations have began (Halls et al., 2000; Peng et al., 2004; Peng, 2005; Wang et al., 2004). Peng et al. (2004) reported major and trace elemental data for the dikes from the Hengshan, Wutai and Fuping metamorphic complexes. Wang et al. (2004) presented a set of geochemical and ^{40}Ar–^{39}Ar geochronological analyses of the mafic dikes from the Zanhuang domain, about 50 km south of the Fuping domain, which is only a small proportion of the Paleoproterozoic unmetamorphosed dikes swarm of the Trans-North China Orogen (Fig. 1b). However, a systematic geochemical study on the mafic dike swarms in the Trans-North China Orogen is lacking, and the nature of the mantle beneath the Trans-North China Orogen during Paleoproterozoic time remains poorly constrained.

In this paper, we conduct a set of geochemical and Sr–Nd isotopic data for the ~1770 Ma mafic dikes from the Sangganhe, Lüliang and Hengshan Mountains to constrain their petrogenesis and the nature of their source. These data are integrated with that from the Zanhuang mafic dikes (Wang et al., 2004) to better understand tectonic processes in the Trans-North China Orogen at ~1800 Ma.

2. Field occurrence and petrology

Two generations of Paleoproterozoic mafic dike swarms in the North China Craton have been identified, with the earlier one metamorphosed in amphibolitic or granulitic facies (e.g. Zhao et al., 2002a,b, 2005; Cooke and O'Brien, 2001; Peng, 2005; Kröner et al., 2006). Zircons separated from two metagabbroic dikes from the Hengshan domain (Dashigou area) yield SHRIMP U–Pb igneous crystallization ages of 1915 ±13 Ma and 1914 ±26 Ma (Kröner et al., 2006), indicating that these dikes were emplaced before the amalgamation of the Eastern and Western Blocks. The mafic dike swarms of the second generation, which are the subject of this study, are devoid of deformation and metamorphism except for minor low-temperature alteration. They are widespread in the Sangganhe, Hengshan, Wutai, Lüliang, Fuping and Zanhuang domains in the Trans-North China Orogen (Fig. 1b), and occasionally exposed in the Eastern and Western Blocks (e.g. Wang et al., 2007). These dikes cut the Achaean and Paleoproterozoic basement rocks, but not the Mesoproterozoic strata (e.g. Changcheng Group).

Well exposed dykes display chilled margins and baked contacts with country rocks. Their width ranges from 1 m to 30 m, locally up to 100 m. Mapped length of individual dikes ranges from 5 to 20 km, with a maximum of ~50 km. Most dikes dip steeply, and have a consistent NW–NNW direction (Figs. 1b and 2a and b), with exception of those in the Lüliang domain where some dikes extend E–W (Figs. 1b and 2c). The major ferromagnesium mineral is augite or ferro-augite, commonly partially altered to chlorite and amphibole. A few samples contain olivine phenocrysts now pseudomorphed by serpentine. Amphibole and relict orthopyroxene lamellae are common. The predominant felsic mineral is plagioclase with andesine-labradorite composition. Plagioclase occurs as phenocrysts and in the groundmass. Minor amounts of quartz, biotite, Fe–Ti oxides and apatite are observed.

These unmetamorphosed dikes in the Trans-North China Orogen have the published crystallization ages of 1781–1765 Ma, based on the following information: (1) an unmetamorphosed doleritic dike from the Hengshan domain yielded a single-grain zircon U–Pb age of 1769.1 ±2.5 Ma (Halls et al., 2000); (2) three representative doleritic dikes from the Zanhuang domain yielded three $^{40}Ar/^{39}Ar$ plateau ages of 1780.7 ±0.5 Ma, 1774.7 ±0.7 Ma and 1765.3 ±1.1 Ma (Wang et al., 2004); (3) a doleritic dike from the west of Fengzhen county gave a SHRIMP U–Pb zircon age of 1778 ±3 Ma (Peng, 2005); (4) similar ages are also obtained from baddeleyites collected from unmetamorphosed dolerites in the Lüliang and Wutai domains (Peng, 2005); and (5) the latest regional metamorphism and ductile deformation have been constrained at 1820–1790 Ma by $^{40}Ar/^{39}Ar$ dating of synkinematic minerals (Wang et al., 2003). Note that the age of the dikes in the Trans-North China Orogen is younger than that of the Eastern Block (1837–1841 Ma, Hou et al., 2006; Wang et al., 2007).

3. Analytical methods

Thirty-five doleritic samples were collected for geochemistry from the Sangganhe (15 samples from the Shanghuangzhuang, Erdaogou, Wulidun-Waoyaokou and Liuyao-Wangyao-Eshi), Lüliang (10 samples from the Miyu and Hengjian) and Hengshan domains (10 samples from the Dongfutou, Dawangcun, Zhongshipu, Hengshanlinchang). The sampling locations are shown in Fig. 2.

Samples were crushed and ground to 200 mesh using an agate mill for elemental and isotopic analyses. Major elements were determined by X-ray fluorescence spectrometry at the Hubei Institute of Geology and Mineral Resource, the Chinese Ministry of Land and Resources. FeO content was analyzed by the wet chemical method. The relative standard derivations (RSD) are within 5%. Trace element abundances were analyzed using an inductively coupled plasma mass spectrometer (ICP-MS) at the Guangzhou Institute of Geochemistry, Chinese Academy of Sciences. The powders (~50 mg) are dissolved in distilled HF-

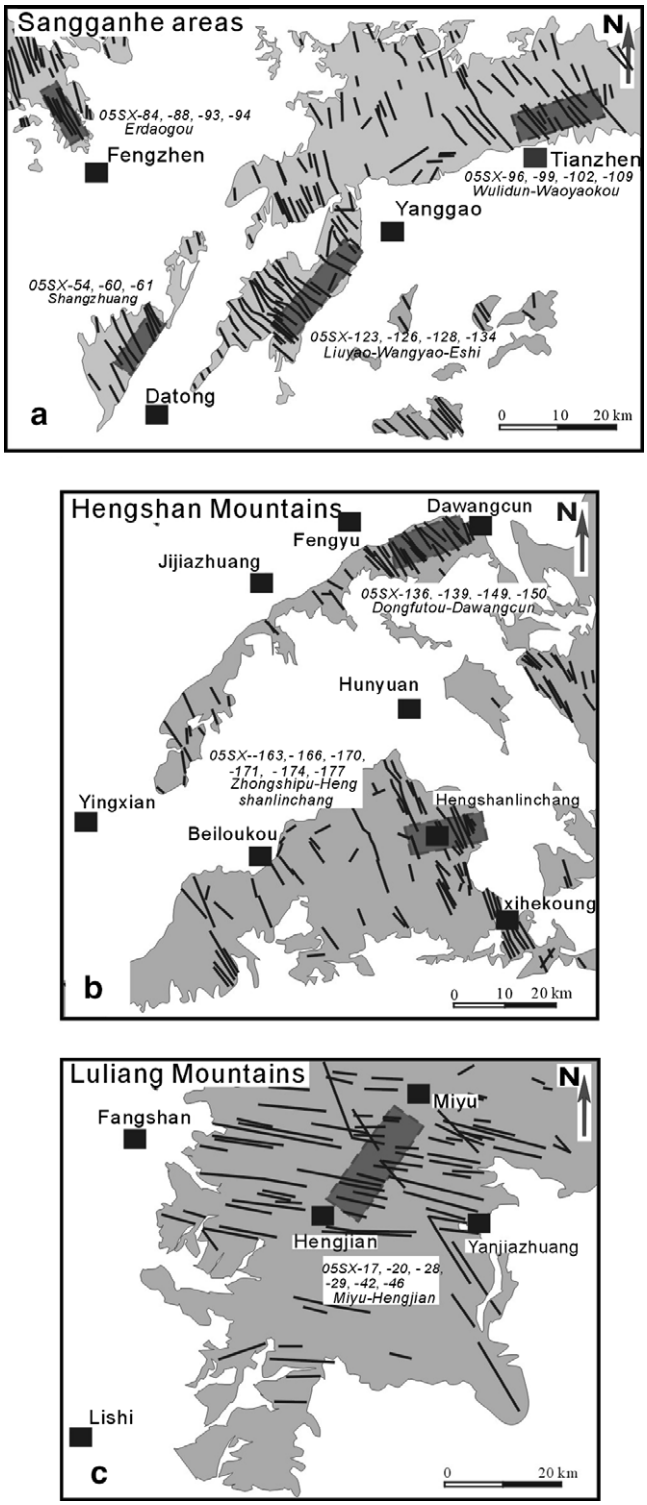

Fig. 2. Geological map showing the distribution of the Paleoproterozoic mafic dikes in the Sangganhe (a), the Hengshan (b) and Lüliang (c) domains. Sampled areas for the analyzed mafic dikes from different areas are shown by shade fields.

HNO_3 in Savillex screwtop Telfon beakers at 150 °C for 4 days. The detailed sample preparation and analytical procedure follow Liu et al. (1996). The reproductivity is better than 95% and the analytical error is <5% for elements >10 ppm, <8% for those <10 ppm, and ~10% for transition metals (Liu et al., 1996). The analytical results are presented in Table 1.

Sr and Nd isotopic ratios were measured by MC–ICP-MS at the Guangzhou Institute of Geochemistry, Chinese Academy of Sciences. Sample preparation and chemical separation are the same as reported by Liang et al. (2003). The total procedure blanks are in the range of 200–500 pg for Sr and less than 50 pg for Nd. Mass fractionation corrections for Sr and Nd isotopic ratios were based on $^{86}Sr/^{88}Sr = 0.1194$ and $^{146}Nd/^{144}Nd = 0.7219$, respectively. The measured $^{87}Sr/^{86}Sr$ ratio of the (NIST) SRM 987 standard and $^{143}Nd/^{144}Nd$ ratio of the La Jolla standard are 0.710265 ± 12 (2σ) and 0.511862 ± 10 (2σ), respectively. Precisions are estimated to be better than 0.000015 for $^{86}Sr/^{88}Sr$ and $^{146}Nd/^{144}Nd$ at the 95% confidence level. Present $^{143}Nd/^{144}Nd$ and $^{147}Sm/^{144}Nd$ ratios of CHUR, 0.512638 and 0.1967, respectively, are used for calculating ε_{Nd} values. $^{87}Rb/^{86}Sr$ and $^{147}Sm/^{144}Nd$ ratios are calculated using the Rb, Sr, Sm and Nd abundances measured by ICP-MS. The measured and age-corrected $^{87}Sr/^{86}Sr$ and $\varepsilon_{Nd}(t)$ are listed in Table 2.

4. Results

The mafic dikes contain have 48.9–56.4% SiO_2 (volatile-free), 2.52–11.20% MgO, 7.86–18.1% FeOt ($= FeO + 0.9 * Fe_2O_3$) and 0.68–3.00% TiO_2. The *mg*-numbers ($= Mg/(Mg + \sum Fe)$ in atomic ratio) vary between 0.20 and 0.69. These rocks fall in the fields of subalkaline basalt and basaltic andesites with exception of two samples (05SX-93 and -94) that fall in the alkaline field with high K_2O contents in the diagram of SiO_2 versus $K_2O + Na_2O$ (LeBas et al., 1986; Fig. 3a). On a plot of Nb/Y versus SiO_2 (Winchester and Floyd, 1977), these samples lie in the fields of basalt and andesite, with an affinity to the subalkaline series (Fig. 3b). These rocks plot in the field of high-Fe tholeiitic rocks in the AFM classification of Jensen (1976). Based on variations in FeOt content, together with the their distinctive $(Nb/La)_N$ and $(Th/La)_N$ ratios, these mafic dikes can be divided into three main groups of Groups 1, 2 and 3 (Fig. 3c), consistent with that proposed by Wang et al. (2004). Such a classification is also applicable for most of the data reported by Peng et al. (2004). Combining the data in Table 1 with the previously published analyses of Wang et al. (2004) and Peng et al. (2004), Group 1 is characterized by high-FeOt contents (12.7–18.1%) and $(Th/La)_N$ ratios (0.60–1.24) but lower $(Nb/La)_N$ ratios (0.18–0.39), and can be classified as basalts and basaltic andesites (Figs. 3a and b). Group 2 has higher $(Nb/La)_N$ ratios (0.64–0.87) in comparison with those of Group 1 in spite of their similar FeOt contents (12.7–16.1%) and $(Th/La)_N$ ratios (0.61–1.20). Group 3 has lower FeOt (7.86–11.6%), varying from subalkaline basalts to andesites and have $(Nb/La)_N$ values of 0.18–0.34 and $(Th/La)_N$ values of 0.29–0.72 (Figs. 3a–c).

At comparable MgO values, Group 1 displays lower Al_2O_3, SiO_2 and higher TiO_2 and P_2O_5 contents than those

Table 1
Major and trace element analyses for the Paleoproterozoic mafic dikes in the Trans-North China Orogen

Sample	05SX-61	05SX-84	05SX-88	05SX-93	05SX-94	05SX-96	05SX-99	05SX-102	05SX-109	05SX-163
	Sangganhe area Group 1									HengShan
Major oxides (wt%)										
SiO_2	51.65	54.21	50.31	49.47	49.78	52.46	52.42	54.29	50.78	54.29
Al_2O_3	12.84	12.62	12.26	11.34	11.29	12.88	12.85	12.95	12.73	12.95
Fe_2O_3	5.79	3.23	0.60	4.60	2.54	3.16	3.60	2.74	4.45	2.74
FeO	8.20	11.45	15.40	13.40	15.50	11.80	11.20	11.00	11.00	11.00
MgO	4.69	3.12	3.64	2.47	2.51	3.33	3.38	3.22	3.69	3.22
CaO	8.91	7.24	8.01	7.00	7.19	7.88	7.80	7.33	7.68	7.33
Na_2O	2.34	2.61	2.38	2.70	2.64	2.55	2.74	2.56	2.44	2.56
K_2O	1.51	1.95	1.96	2.39	2.31	1.84	1.83	2.19	2.18	2.19
MnO	0.21	0.22	0.24	0.26	0.26	0.22	0.21	0.20	0.22	0.20
TiO_2	1.05	1.56	2.62	2.95	2.93	2.29	2.33	1.64	2.53	1.64
P_2O_5	0.14	0.42	1.03	1.59	1.52	0.40	0.40	0.47	0.95	0.47
LOI	2.48	1.10	1.23	1.51	1.23	0.95	1.00	1.13	1.03	1.13
Total	99.81	99.73	99.68	99.68	99.70	99.76	99.76	99.72	99.68	99.72
FeOt	13.41	14.36	15.94	17.54	17.79	14.64	14.44	13.47	15.01	13.47
$mg^{\#}$	0.39	0.28	0.29	0.20	0.20	0.29	0.30	0.30	0.31	0.30
Trace elements (ppm)										
Sc	46.3	32.7	32.2	28.9	29.3	30.4	30.6	30.6	28.3	37.8
V	312	318	208	39	31	251	255	288	281	324
Cr	62.6	4.9	41.2	2.8	3.5	57.4	52.5	12.2	21.3	16.1
Co	53.7	43.5	35.5	31.8	31.0	37.9	38.7	41.0	40.6	39.9
Ni	50.5	8.4	23.2	2.4	3.3	36.2	36.0	13.3	14.8	19.7
Rb	12.6	46.9	41.5	56.2	55.7	53.3	50.9	52.1	35.5	39.2
Sr	222	355	338	366	374	273	276	336	380	298
Y	23.0	32.4	43.4	54.1	53.3	48.2	45.6	32.3	32.6	44.7
Zr	78	185	203	357	350	347	346	193	192	156
Nb	2.73	7.87	11.30	20.96	20.82	19.04	18.03	8.73	9.03	8.03
Ba	186	1008	1568	1551	1586	1503	1683	1097	1361	1142
La	8.49	39.57	45.87	63.04	60.23	45.44	44.93	43.32	43.03	39.72
Ce	19.40	80.73	97.26	130.9	128.5	96.54	91.65	85.33	87.79	83.47
Pr	2.82	10.05	13.04	19.24	18.39	12.76	12.33	10.67	11.84	11.39
Nd	12.48	43.03	59.60	83.32	82.16	54.81	50.84	44.61	49.54	51.11
Sm	3.13	7.58	10.99	16.11	15.20	10.58	10.27	7.78	8.90	9.67
Eu	1.08	2.10	3.57	4.99	4.92	2.64	2.48	2.13	2.77	2.97
Gd	3.46	6.88	10.04	14.29	13.70	10.01	9.57	7.03	7.89	9.18
Tb	0.68	1.09	1.57	2.07	2.08	1.71	1.56	1.14	1.16	1.52
Dy	4.32	6.07	8.26	11.06	10.55	9.47	8.98	5.99	6.55	8.51
Ho	0.86	1.21	1.61	1.98	1.96	1.86	1.68	1.22	1.22	1.70
Er	2.41	3.30	4.18	4.94	4.83	4.80	4.51	3.20	3.26	4.54
Tm	0.38	0.48	0.60	0.70	0.69	0.74	0.68	0.49	0.49	0.70
Yb	2.49	3.30	3.88	4.43	4.31	4.67	4.34	3.26	3.06	4.54
Lu	0.38	0.54	0.63	0.68	0.67	0.74	0.68	0.51	0.48	0.75
Hf	2.01	4.77	4.98	7.40	7.14	7.44	7.13	4.84	4.52	4.42
Ta	0.20	0.53	0.78	1.42	1.36	1.31	1.22	0.58	0.55	0.55
Pb	2.83	10.89	8.89	10.92	10.47	10.58	10.56	11.26	9.59	8.39
Th	0.96	5.56	4.46	6.13	5.84	5.58	5.47	5.72	3.20	3.68
U	0.25	1.08	0.76	1.14	1.13	0.93	0.89	1.00	0.50	0.75
$(Nb/La)_N$	0.31	0.19	0.24	0.32	0.33	0.40	0.39	0.19	0.20	0.19
$(Nb/Zr)_N$	0.55	0.67	0.87	0.92	0.93	0.86	0.82	0.71	0.74	0.81
$(Th/La)_N$	0.91	1.14	0.79	0.79	0.78	0.99	0.98	1.07	0.65	0.75
$(Hf/Sm)_N$	0.93	0.90	0.65	0.66	0.67	1.01	1.00	0.89	0.73	0.66
(La/Yb)cn	2.31	8.10	7.98	9.61	9.45	6.57	7.00	8.99	9.51	5.91
(Gd/Yb)cn	1.13	1.69	2.10	2.61	2.58	1.74	1.79	1.75	2.09	1.64
Eu/Eu^*	1.00	0.88	1.02	0.99	1.02	0.77	0.75	0.87	0.99	0.95

Sample	05SX-166	05SX-170	05SX-171	05SX-174	05SX-177	05SX-123	05SX126	05SX-128	05SX-149	05SX-150
	Hengs Shan Group 1					Sangganhe area Group 2			Heng Shan	
Major oxides (wt%)										
SiO_2	50.75	50.69	50.59	51.27	54.14	49.28	47.97	49.09	48.06	49.15

(*continued on next page*)

Table 1 (*continued*)

Sample	05SX-166	05SX-170	05SX-171	05SX-174	05SX-177	05SX-123	05SX126	05SX-128	05SX-149	05SX-150
	Hengs Shan Group 1					Sangganhe area Group 2			Heng Shan	
Al_2O_3	11.99	11.97	11.95	12.11	13.56	12.03	11.63	11.78	12.31	13.13
Fe_2O_3	3.23	3.00	3.13	2.69	2.33	4.53	4.79	4.15	4.23	4.76
FeO	13.60	13.80	13.70	13.65	10.50	10.90	11.15	11.60	11.50	10.50
MgO	3.45	3.42	3.49	3.15	4.18	4.54	4.69	4.75	5.72	4.47
CaO	8.02	8.10	8.05	7.80	8.41	8.59	8.65	8.56	10.61	9.39
Na_2O	2.25	2.33	2.31	2.29	2.56	2.05	2.03	2.24	1.72	2.08
K_2O	1.77	1.81	1.80	1.97	1.58	1.70	1.86	1.90	1.27	1.69
MnO	0.25	0.24	0.25	0.24	0.20	0.24	0.25	0.24	0.24	0.23
TiO_2	2.53	2.56	2.53	2.60	1.16	2.38	2.56	2.43	2.45	2.46
P_2O_5	0.77	0.79	0.78	0.95	0.33	0.26	0.24	0.23	0.14	0.20
LOI	1.09	1.01	1.13	1.01	0.82	3.28	3.94	2.81	1.54	1.74
Total	99.70	99.72	99.71	99.73	99.77	99.78	99.76	99.78	99.79	99.80
FeOt	16.51	16.50	16.52	16.07	12.60	14.98	15.46	15.34	15.31	14.78
$mg^{\#}$	0.27	0.27	0.28	0.26	0.37	0.35	0.35	0.36	0.40	0.35
Trace elements (ppm)										
Sc	38.2	36.0	36.1	32.2	30.1	41.2	41.5	38.2	44.6	38.0
V	352	325	309	234	216	421	501	428	597	437
Cr	16.8	23.0	16.6	3.8	8.8	80.3	75.0	78.4	93.7	69.9
Co	40.0	38.6	39.2	35.5	41.0	45.4	49.3	46.0	54.3	48.3
Ni	18.1	23.1	18.5	10.5	21.1	55.8	60.3	53.6	74.8	52.7
Rb	36.3	39.2	36.2	42.2	35.6	18.1	24.4	21.0	6.9	33.0
Sr	291	305	292	300	359	234	282	245	128	164
Y	41.1	43.3	42.2	44.8	24.9	42.8	40.3	40.4	24.3	34.1
Zr	171	175	176	184	139	177	169	175	92	143
Nb	7.38	7.93	7.48	8.36	6.07	12.95	11.71	12.35	6.68	9.97
Ba	1069	1101	1055	1153	808	147	190	182	81	170
La	36.90	38.93	37.92	42.82	30.58	16.42	15.14	15.71	8.50	13.05
Ce	78.94	83.95	79.63	90.06	60.98	38.36	35.93	36.00	19.91	29.03
Pr	11.00	11.26	10.99	12.44	7.81	5.46	5.11	5.19	2.89	4.37
Nd	48.15	50.23	47.94	53.29	32.10	26.35	24.42	25.88	13.62	20.46
Sm	9.51	9.80	9.46	10.27	5.91	6.32	5.93	7.20	3.58	5.02
Eu	2.77	2.89	2.80	3.02	1.66	2.02	1.91	1.94	1.23	1.65
Gd	8.99	9.27	9.05	9.44	5.53	6.85	6.41	6.42	3.89	5.40
Tb	1.50	1.51	1.47	1.51	0.88	1.34	1.27	1.27	0.78	1.06
Dy	8.58	8.49	8.48	8.76	5.05	7.81	7.29	7.49	4.70	6.40
Ho	1.67	1.69	1.63	1.69	0.97	1.59	1.51	1.52	0.93	1.31
Er	4.55	4.52	4.46	4.59	2.70	4.22	3.96	4.00	2.51	3.39
Tm	0.67	0.67	0.68	0.70	0.40	0.65	0.61	0.63	0.39	0.55
Yb	4.48	4.49	4.42	4.51	2.65	4.32	4.11	4.11	2.57	3.55
Lu	0.71	0.72	0.70	0.73	0.41	0.69	0.67	0.66	0.40	0.59
Hf	4.82	4.75	4.65	4.90	3.58	4.46	4.38	4.49	2.47	3.72
Ta	0.54	0.55	0.52	0.60	0.40	0.92	0.85	0.89	0.49	0.75
Pb	8.35	8.38	8.13	8.98	8.66	3.28	2.20	1.98	2.11	3.70
Th	3.77	3.96	3.67	4.32	4.11	2.38	2.05	2.32	1.05	1.85
U	0.82	0.84	0.77	0.87	0.74	0.54	0.47	0.51	0.26	0.49
$(Nb/La)_N$	0.19	0.20	0.19	0.19	0.19	0.76	0.75	0.76	0.76	0.74
$(Nb/Zr)_N$	0.68	0.71	0.67	0.71	0.69	1.15	1.09	1.11	1.14	1.10
$(Th/La)_N$	0.83	0.82	0.78	0.82	1.09	1.17	1.10	1.19	1.00	1.15
$(Hf/Sm)_N$	0.73	0.70	0.71	0.69	0.87	1.01	1.06	1.29	0.99	1.06
(La/Yb)cn	5.57	5.86	5.80	6.41	7.79	2.57	2.49	2.58	2.24	2.48
(Gd/Yb)cn	1.63	1.67	1.66	1.69	1.69	1.28	1.26	1.26	1.23	1.23
Eu/Eu^*	0.90	0.91	0.91	0.92	0.88	0.94	0.94	0.96	1.00	0.96
Sample	05SX-54	05SX-60	05SX-134	05SX-136	05SX-139	05SX-17	05SX-20	05SX-29	05SX42	05SX-46
	Sangganhe area Group 3					Lüliang Shan				
Major oxides (wt%)										
SiO_2	50.89	49.59	51.33	51.69	51.73	50.24	50.46	55.45	54.64	55.02
Al_2O_3	13.57	16.31	15.38	15.38	15.96	14.32	14.39	14.75	14.73	14.60
Fe_2O_3	3.97	5.55	2.13	1.23	1.06	2.63	2.08	2.92	2.77	2.61
FeO	7.35	6.40	9.50	10.10	9.25	8.90	8.55	7.00	7.70	7.90

Table 1 (*continued*)

Sample	05SX-54	05SX-60	05SX-134	05SX-136	05SX-139	05SX-17	05SX-20	05SX-29	05SX42	05SX-46
	Sangganhe area Group 3					Lüliang Shan				
MgO	5.58	6.17	5.70	5.96	6.14	6.49	6.61	4.09	3.95	3.54
CaO	9.40	7.78	9.58	9.69	10.33	10.75	10.37	7.04	7.24	6.61
Na_2O	2.31	3.35	2.38	2.34	2.37	1.99	2.4	2.79	2.22	2.62
K_2O	1.43	0.81	1.15	1.09	0.88	0.92	1.17	1.58	2.75	2.88
MnO	0.18	0.13	0.18	0.18	0.18	0.20	0.20	0.17	0.18	0.16
TiO_2	1.42	1.00	0.90	0.84	0.67	0.93	0.71	1.00	1.11	1.24
P_2O_5	0.23	0.23	0.24	0.22	0.17	0.13	0.10	0.26	0.29	0.36
LOI	3.14	2.44	1.25	1.02	1.02	2.32	2.79	2.68	2.16	2.15
Total	99.57	99.76	99.72	99.74	99.76	99.82	99.83	99.73	99.74	99.69
FeOt	10.92	11.40	11.42	11.21	10.20	11.27	10.42	9.63	10.19	10.25
$mg^{\#}$	0.48	0.49	0.47	0.49	0.52	0.51	0.53	0.43	0.41	0.38
Trace elements (ppm)										
Sc	40.1	26.0	29.5	28.1	30.5	36.8	41.2	22.8	23.7	22.8
V	287	182	193	182	178	234	223	131	140	134
Cr	36.4	72.5	64.1	74.1	73.0	218.4	140.9	166.8	148.1	130.5
Co	41.5	46.5	42.2	45.2	45.4	49.5	45.2	31.4	30.2	28.7
Ni	27.9	99.8	60.2	65.2	72.4	113.7	67.1	44.8	71.6	40.1
Rb	31.2	11.0	19.1	17.5	14.3	84.7	85.9	33.7	310.8	157.2
Sr	326	482	458	442	476	221	238	439	377	400
Y	35.7	20.0	19.3	18.1	15.2	21.7	16.6	28.0	35.4	35.2
Zr	143	73	93	80	62	77	50	140	156	201
Nb	6.34	3.81	3.73	3.35	2.71	2.94	1.90	5.96	6.59	8.50
Ba	902	368	812	711	626	181	200	1117	1175	1385
La	29.17	12.92	19.25	17.84	14.28	9.06	6.18	30.48	33.50	41.76
Ce	60.66	30.11	40.61	36.31	30.80	20.30	13.95	60.87	67.92	85.83
Pr	8.57	4.17	5.42	4.97	4.03	2.78	1.94	8.23	9.00	11.18
Nd	37.46	19.14	23.36	20.96	17.67	12.84	9.08	33.29	38.77	46.37
Sm	7.45	4.10	4.56	4.07	3.34	2.86	2.19	6.22	7.07	8.30
Eu	2.43	1.28	1.41	1.32	1.12	1.02	0.79	1.64	1.87	2.04
Gd	7.15	3.63	4.11	3.73	3.12	3.22	2.44	5.58	6.60	7.48
Tb	1.18	0.64	0.68	0.58	0.52	0.64	0.49	0.90	1.10	1.20
Dy	6.77	3.56	3.74	3.44	2.94	3.84	3.01	5.20	6.11	6.67
Ho	1.36	0.72	0.73	0.67	0.57	0.82	0.63	1.04	1.22	1.30
Er	3.64	2.00	1.97	1.81	1.59	2.24	1.70	2.78	3.38	3.66
Tm	0.59	0.29	0.31	0.30	0.24	0.33	0.26	0.45	0.50	0.55
Yb	3.70	1.99	2.07	1.94	1.63	2.26	1.74	2.99	3.34	3.64
Lu	0.61	0.32	0.33	0.31	0.26	0.36	0.29	0.49	0.55	0.58
Hf	3.79	1.92	2.46	2.11	1.68	1.91	1.35	3.67	4.00	5.12
Ta	0.45	0.25	0.25	0.22	0.19	0.21	0.13	0.38	0.42	0.52
Pb	6.85	3.37	5.44	4.53	4.18	3.40	4.04	9.00	26.42	21.35
Th	2.37	0.53	1.69	1.63	1.37	0.65	0.53	2.03	1.79	2.46
U	0.59	0.09	0.34	0.29	0.25	0.21	0.12	0.39	0.38	0.56
$(Nb/La)_N$	0.21	0.28	0.19	0.18	0.18	0.31	0.30	0.19	0.19	0.20
$(Nb/Zr)_N$	0.70	0.82	0.63	0.66	0.69	0.60	0.60	0.67	0.66	0.66
$(Th/La)_N$	0.64	0.33	0.71	0.74	0.77	0.62	0.69	0.54	0.43	0.48
$(Hf/Sm)_N$	0.73	0.71	0.78	0.75	0.72	0.96	0.88	0.85	0.81	0.89
(La/Yb)cn	5.32	4.40	6.28	6.22	5.92	2.71	2.40	6.89	6.79	7.75
(Gd/Yb)cn	1.56	1.48	1.61	1.56	1.55	1.15	1.14	1.51	1.60	1.66
Eu/Eu^*	1.00	1.02	0.98	1.02	1.04	1.03	1.04	0.83	0.82	0.78

Detailed sampling locations for each sample can be labeled in Fig. 2. $FeOt = FeO + 0.9 * Fe_2O_3$, LOI: loss on ignition, *mg*-number $= Mg^{2+}/(Mg^{2+} + Fe^{2+})$, $Eu/Eu^* = (Eu)cn/[(Gd)cn + (Sm)cn]/2$, Symbol with "cn" denotes the values normalized to chondrite, and with "N" denotes values normalized against primitive mantle.

of Group 3 but similar contents of major oxides and compatible elements to those of Group 2 (Table 1 and Figs. 4a–d). In the Harker diagrams (Figs. 4a–e), MgO inversely correlates with SiO_2, P_2O_5 and TiO_2, but positively with Al_2O_3, CaO, Ni and Cr for Groups 1 and 3. Similarly, incompatible elements (e.g. Th, Ba, La, Gd, Y and Nb) with the exception of Sr drastically increase with decrease in MgO (Figs. 4f–h). The limited range of major oxide values in Group 2 prevents the recognition of any trends (Fig. 4).

The incompatible element compositions exhibit distinct variations among these groups (Table 1). The light

Table 2
Sr–Nd isotopic analyses for the Paleoproterozoic mafic dikes in the Trans-North China Orogen

Sample	Sm	Nd	Rb	Sr	$^{147}Sm/^{144}Nd$	$^{87}Rb/^{86}Sr$	$^{143}Nd/^{144}Nd$ (2σ)	$^{87}Sr/^{86}Sr$ (2σ)	$^{87}Sr/^{86}Sr(t)$	$\varepsilon_{Nd}(t)$
Group 1										
05SX-88	10.99	59.60	41.53	337.70	0.112	0.357	0.511472 (8)	0.712932 (18)	0.70396	−3.6
05SX-93	16.11	83.32	56.22	365.90	0.117	0.445	0.511596 (6)	0.715345 (16)	0.70414	−2.4
05SX-102	7.78	44.61	52.05	336.20	0.105	0.449	0.511359 (8)	0.715895 (23)	0.70460	−4.5
05SX-109	8.90	49.54	35.48	380.40	0.109	0.270	0.511382 (7)	0.712639 (14)	0.70584	−4.8
05SX-166	9.51	48.15	36.30	291.30	0.119	0.361	0.511484 (6)	0.713748 (16)	0.70466	−5.2
05SX-171	9.46	47.94	36.20	291.90	0.119	0.360	0.511557 (7)	0.713929 (13)	0.70488	−3.7
99JX-62[a]	4.84	18.17	5.78	246.0	0.161	0.068	0.511985 (11)	0.706232 (17)	0.70453	−4.8
99JX-69[a]	4.15	16.49	11.76	193.0	0.152	0.177	0.511954 (6)	0.709722 (17)	0.70528	−3.4
99JX-70[a]	4.28	17.87	9.17	244.1	0.145	0.109	0.511797 (10)	0.707769 (13)	0.70503	−4.8
99JX-76[a]	5.59	21.08	3.99	203.2	0.160	0.057	0.511956 (8)	0.706528 (14)	0.70509	−5.1
Group 2										
05SX-128	7.20	25.88	21.04	245.30	0.168	0.249	0.512366 (7)	0.709648 (21)	0.70339	1.1
05SX-149	3.58	13.62	6.90	128.2	0.159	0.156	0.512152 (8)	0.707196 (20)	0.70327	−1.0
99JX-16[a]	3.09	10.00	15.21	166.3	0.187	0.265	0.512436 (10)	0.712056 (14)	0.70539	−1.7
99JX-18[a]	3.76	12.32	22.07	174.1	0.184	0.368	0.512414 (9)	0.714497 (15)	0.70525	−1.6
99JX-20[a]	3.46	12.11	30.47	229.6	0.173	0.385	0.512292 (10)	0.714934 (17)	0.70525	−1.5
99JX-81[a]	3.10	10.38	4.98	178.4	0.181	0.081	0.512422 (11)	0.706673 (17)	0.70464	−0.6
99JX-87[a]	3.08	10.36	20.46	119.0	0.180	0.499	0.512385 (10)	0.717161 (17)	0.70462	−1.2
Group 3										
05SX-20	12.57	74.36	117.2	432.10	0.102	0.786	0.511350 (6)	0.72468 (16)	0.70485	−3.9
05SX-29	10.68	61.43	64.05	447.30	0.105	0.415	0.511349 (6)	0.714844 (14)	0.70440	−4.6
05SX-46	13.45	78.66	66.01	375.10	0.103	0.510	0.511341 (7)	0.717174 (13)	0.70434	−4.4
05SX-54	7.45	37.46	31.17	326.10	0.120	0.277	0.511684 (7)	0.711407 (16)	0.70443	−1.4
05SX-60	4.10	19.14	11.03	482.00	0.130	0.066	0.511804 (7)	0.70546 (13)	0.70379	−1.2
05SX-136	4.07	20.96	17.53	441.70	0.117	0.115	0.511618 (7)	0.706785 (16)	0.70389	−2.1
05SX-139	3.34	17.67	14.28	476.10	0.114	0.087	0.511570 (8)	0.706338 (14)	0.70415	−2.4
99JX-02[a]	5.13	24.49	6.75	361.2	0.127	0.054	0.511668 (8)	0.705326 (16)	0.70402	−3.2
99JX-04[a]	5.26	24.80	8.00	359.8	0.128	0.064	0.511643 (8)	0.705783 (11)	0.70425	−4.1
99JX-07[a]	4.53	22.04	4.08	327.8	0.124	0.036	0.511665 (8)	0.704993 (16)	0.70411	−2.8
99JX-54[a]	4.43	21.16	31.35	373.7	0.127	0.243	0.511664 (11)	0.711091 (9)	0.70499	−3.3
99JX-56[a]	2.87	11.80	33.13	300.0	0.147	0.320	0.511785 (9)	0.712802 (13)	0.70475	−5.5
99JX-58[a]	3.69	16.18	10.19	392.9	0.138	0.075	0.511703 (9)	0.706326 (13)	0.70445	−5.1

[a] Samples from Wang et al. (2004).

rare-earth elements (LREEs) of Groups 1 and 3 are moderately to highly fractionated relative to the heavy rare-earth elements (HREEs) with (La/Yb)cn = 2.3–10.9 (Figs. 5a and c) and $Eu/Eu^* = 0.75–1.11$. (Gd/Yb)cn ratios range from 1.1 for 2.8. In contrast, Group 2 has (La/Yb)cn = 1.4–2.6 and (Gd/Yb)cn = 0.9–1.3, showing a flat REE pattern, with $Eu/Eu^* = 0.90–1.06$ (Table 1 and Fig. 5b). On the primitive-mantle normalized spidergram (Figs. 5d–f), Group 1 shows subparallel "spiky" patterns with deep Nb–Ta and variable Sr, Ti and Zr–Hf troughs. Such characteristics are similar to those of island arc volcanic rocks. Group 2 has relatively flat patterns with no Th–U, Nb–Ta and P–Ti anomalies. Group 3 exhibits Nb–Ta, Ti and Zr–Hf negative anomalies. Other striking features among the three groups are the magnitude of Nb–Ta and Th–U anomalies. Groups 1 and 3 have $(Nb/La)_N$ ratio of 0.16–0.39, significantly lower than that of Group 2 (0.65–0.86). Group 1 shows a depletion of Th and U relative to La, with $(Th/La)_N = 0.56–1.27$, similar to that of Group 2 (0.61–1.20), but significantly higher than that of Group 3 ($(Th/La)_N = 0.29–0.74$).

The initial Sr isotopic ratios range from 0.70327 to 0.70584, and $\varepsilon_{Nd}(t)$ values vary from 1.1 to −5.5 for all these samples in the Trans-North China Orogen (Table 2), exhibiting an affinity to an EMI-like source (Fig. 6). Group 1 has $\varepsilon_{Nd}(t)$ values of −2.4 to −5.2, similar to those of Group 3 (−1.2 to −5.5), but lower than those of Group 2 (1.1 to −1.7). The isotopic compositions are generally similar to or slight higher than those of the synchronous Xiong'er volcanic rocks in the southern margin of the North China Craton ($\varepsilon_{Nd}(t) = -3.8$ to −9.0, Zhao et al., 2002a,b).

5. Discussion

5.1. Magma fractionation?

Most mafic dikes in the region do not represent primary melts, as indicated by their low MgO (mostly <8.0%), *mg*-number (0.20–0.69) and Ni contents (2–338 ppm). Their precursor magmas must have undergone variable degrees of fractional crystallization in the magma chambers prior to their emplacement. As shown in Fig. 4, Groups 1 and 3 have distinctive magma evolution trends, while Group 2 has a relatively limited variation of major oxides. This, together with the distinctive ratios of incom-

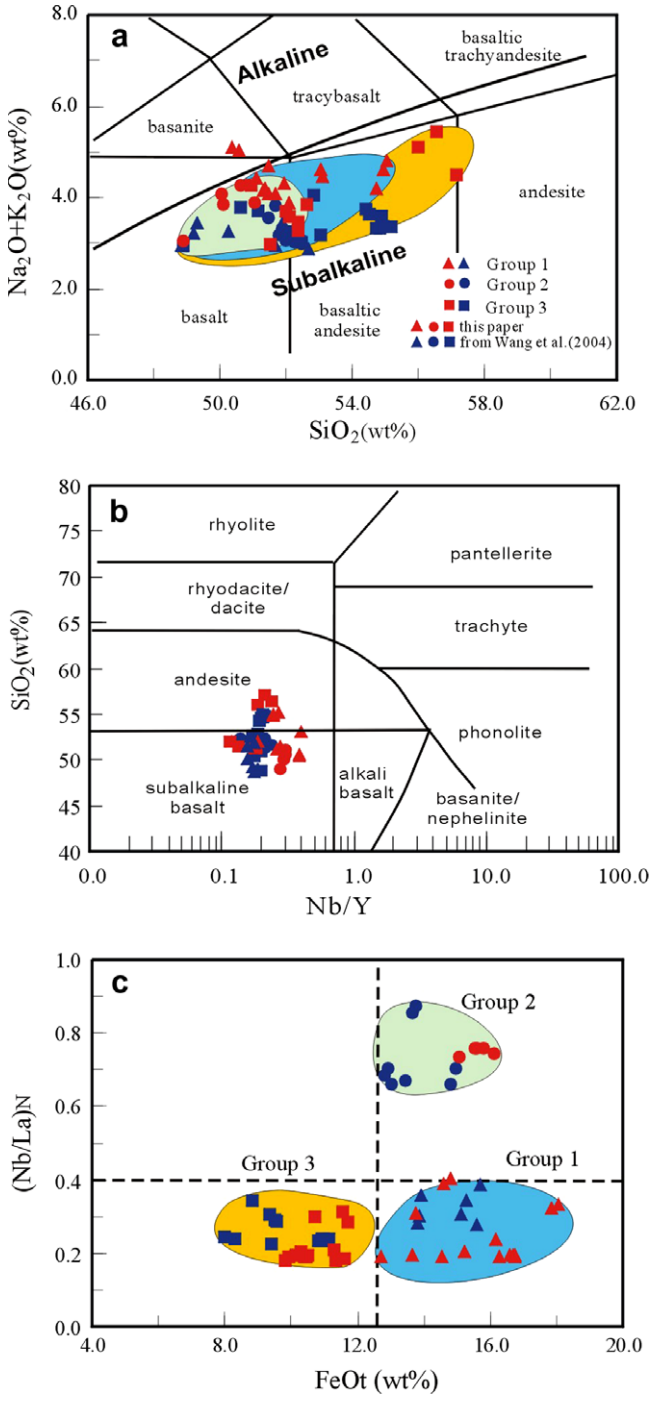

Fig. 3. (a) SiO_2 versus $K_2O + Na_2O$, (b) Nb/Y versus SiO_2, (c) FeOt (= FeO + 0.9 * Fe_2O_3) versus $(Nb/La)_N$. (a) and (b) are after LeBas et al. (1986), and Winchester and Floyd (1977), respectively. Symbols in (b–c) are the same as in (a).

patible elements and isotopic compositions (Tables 1 and 2), suggests that these groups may have come from different magma chambers.

For Groups 1 and 3, the relationships of MgO and SiO_2, CaO and Al_2O_3 (Figs. 4a–c) are consistent with fractional crystallization involving clinopyroxene ± plagioclase. Negative correlations of MgO and P_2O_5 (not shown), and TiO_2 (Fig. 4d) indicate that fractionation of apatite and magnetite is likely insignificant. Thus, the P–Ti depletions in some samples (Figs. 5d–f) may reflect the characteristics of the source rather than the result of apatite and Ti–Fe-oxides fractionation. The decrease of Ni, Cr and Co contents with the magma evolution indicates the importance of olivine and clinopyroxene fractionation (Fig. 4e). With the exception of Group 3 rocks with $SiO_2 > 55$ wt%, most samples have undergone little plagioclase fractionation, as reflected by the subparallel REE patterns, weak Eu anomalies and irregular variation in Eu/Eu^* with increasing SiO_2.

It is more difficult to evaluate the role of fractional crystallization for Group 2 rocks because of their narrow compositional range, although clinopyroxene fractionation is possible as MgO appears to be well correlated with CaO and Al_2O_3 (Figs. 4a and c). These samples have low *mg*-number (0.35–0.50) and compatible element contents, which are indicative of a significant differentiation. Plagioclase fractionation should be insignificant for Group 2, as reflected by slight Sr and Eu/Eu^* anomalies (Figs. 5b and e). However, a simple fractional crystallization fractionation process cannot reconcile the variable incompatible element ratios and "crustal" isotopic characteristics of the samples (Tables 1 and 2). FeOt is positively correlated with $\varepsilon_{Nd}(t)$ for these groups (Fig. 7a), which is also inconsistent with the process of fractional crystallization.

5.2. Crustal contamination during magma ascent?

In the case of Group 1, the following characteristics appear to argue against significant crustal assimilation during magmatic differentiation: (1) FeOt (>12.5%) and TiO_2 (>1.5% for most samples) are higher than those of the upper crust of the North China Craton (Zhang et al., 1994) and the average continental crust (Rudnick and Fountain, 1995); (2) $(Nb/La)_N$ ratios (0.16–0.39) are lower than those of the lower crust of the North China Craton (Gao et al., 1998; Zhang et al., 1994) and the average crust (Rudnick and Fountain, 1995; Taylor and McLennan, 1985); (3) $(Nb/La)_N$ values are relatively constant and $(Th/La)_N$ ratios vary irregularly with SiO_2 content; and (4) $\varepsilon_{Nd}(t)$ values generally increase with magma evolution.

It is generally known that the crustal contamination during magma ascent will result in an increase in LREE and LILE and a decrease in $\varepsilon_{Nd}(t)$ value. However, this is not the case for Group 2 (Tables 1 and 2). Minimal crustal contamination during magmatic differentiation is also supported for Group 2 by the following observations: (1) Group 2 exhibits flat REE patterns and high-FeOt content of >12.5%; (2) $(Nb/La)_N$ ratios are in the range of 0.64–0.87, and show an insignificant correlation with SiO_2; (3) $\varepsilon_{Nd}(t)$ values generally increase with decrease in *mg*-number.

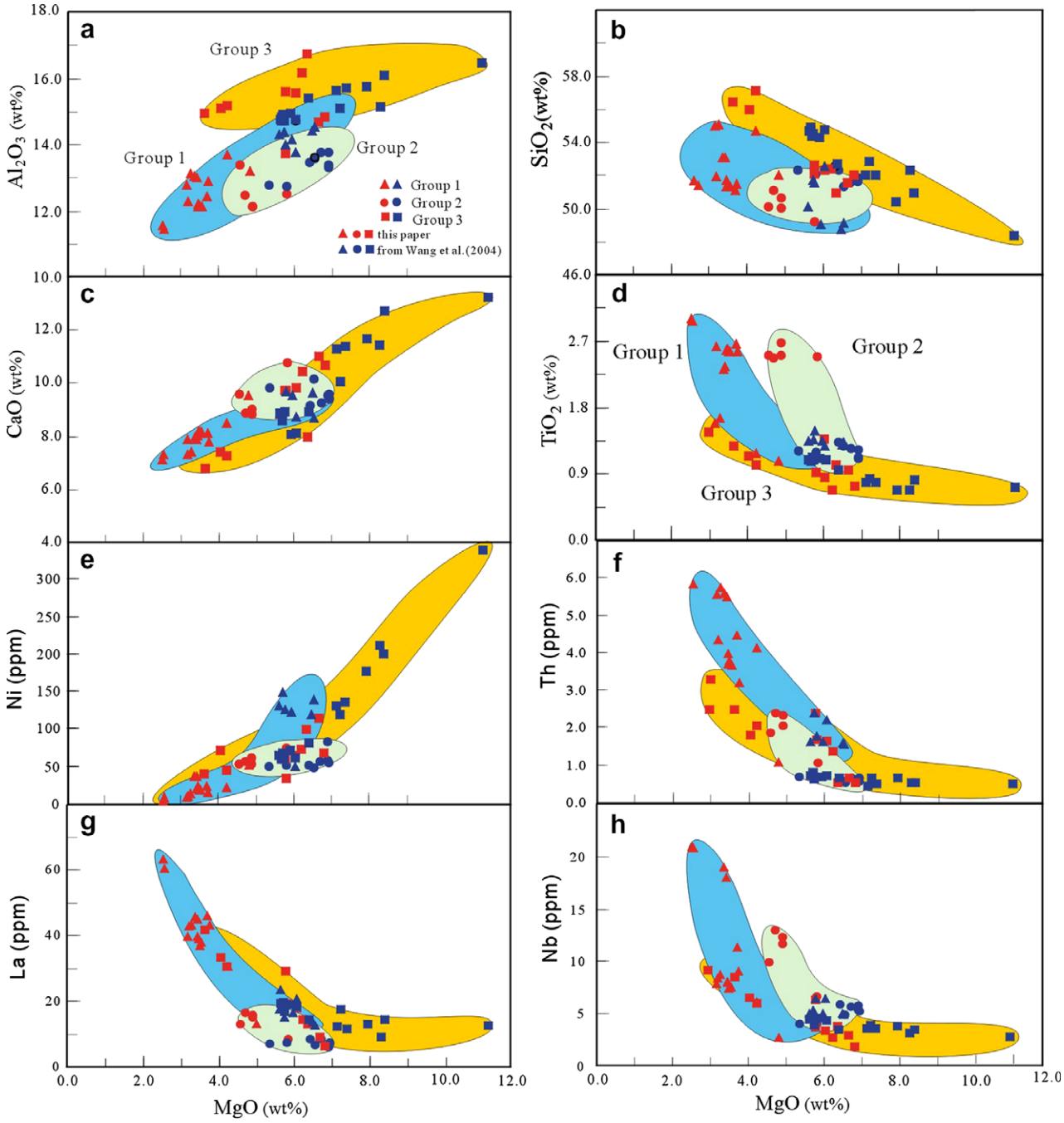

Fig. 4. Plots of MgO versus Al_2O_3 (a), SiO_2 (b), CaO (c), TiO_2(d), Ni (e), Th (f), La (g) and Nb (h) for the ~1770 Ma mafic dikes in the Trans-North China Orogen. All major oxides are normalized to 100% on a volatile-free basis. Symbols are the same as those in (a).

Group 3 has low Th and U contents, with Th/La ratios of 0.29–0.72, $(Nb/La)_N$ ratios of 0.18–0.34, and slightly variable $(Th/La)_N$ and $(Nb/La)_N$ ratios irrespective of SiO_2. The samples show an inverse correlation between *mg*-number and $\varepsilon_{Nd}(t)$ value, which could not be explained by significant crustal assimilation and fractionated crystallization. The broad similarity of immobile incompatible element behavior (e.g. subparallel REE pattern) also suggests a negligible crustal contamination during magma assent. Therefore, the variability of elemental and isotopic compositions for each group more likely indicates the nature of source region rather than crustal assimilation.

5.3. Characteristics of the source regions

In order to minimize the effect of partial melting and fractional crystallization processes, the isotopic compositions and ratios of incompatible elements with similar distribution coefficients (e.g. Th/La, Zr/Nb, Nb/La, Nb/Y and Th/Ba) are used to probe into the source characteristics of these samples.

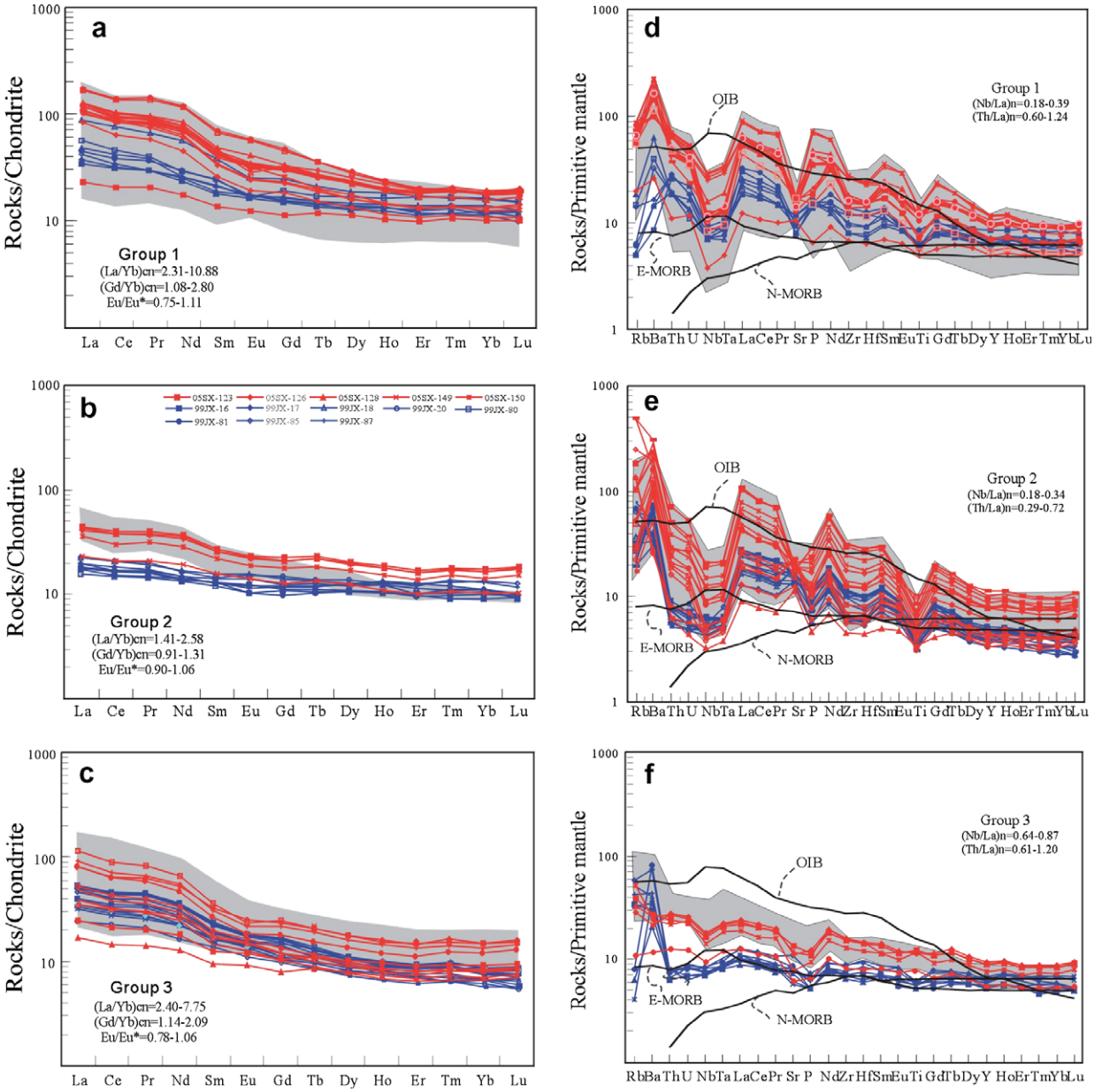

Fig. 5. Chondrite-normalized REE patterns (a–c) and primitive-mantle normalized trace element patterns (d–f) for the 1765–1781 Ma mafic dikes in the Trans-North China Orogen. (a) REE pattern for Group 1; (b) REE pattern for Group 2; (c) REE pattern for Group 3; (d) PM pattern for Group 1; (e) PM pattern for Group 2; (f) PM pattern for Group 3. Normalized values for chondrite in (a–c) are from Taylor and McLennan (1985). Shaded data are from Peng (2005). (La/Yb)cn and (Gd/Yb)cn are normalized to Chondrite. Normalizing values, and OIB, N-MORB and E-MORB fields in (d–f) are from Sun and Mcdonough (1989). Shaded data are from Peng (2005). $(Nb/La)_N$ and $(Th/La)_N$ values are normalized against primitive mantle.

5.3.1. Groups 1 and 3

Groups 1 and 3 rocks are characterized by enrichment in LILEs and LREEs, depletion in HFSEs, and low $\varepsilon_{Nd}(t)$ values and $(Nb/La)_N$ and $(Nb/Zr)_N$ ratios (Tables 1 and 2). These characteristics are similar to those of arc volcanics and suggest an involvement of an "old" continental component in the source. Consequently, it argues for an origin from subduction-related lithospheric mantle (Wang et al., 2004). Positive correlation of MgO with Al_2O_3 and CaO for both groups (Figs. 4a and c) suggest that the primitive magma might have relatively high Al_2O_3 and CaO contents, indicative of high clinopyroxene/orthopyroxene ratios in the source, which may have resulted from metasomatism of peridotites by carbonatitic- or subduction-melt/fluid (Kogarko et al., 2001; Yaxley et al., 1998). However, a melt from a carbonate-metasomatised source is commonly ultramafic, depleted in Al_2O_3 (Gasparik and Litvin, 2002; Hammouda, 2003), and has a strong depletion in HFSEs relative to REEs (LaFlèche et al., 1998). This is in contrary to the observation that both groups are subalkaline basalt with high Al_2O_3 and CaO contents, and are characterized by high $(Hf/Sm)_N$ and low $(Ta/Th)_N$ ratios. These mafic dikes plot in the field of subduction-related metasomatism in Fig. 7b. Generally, metasomatism related to SiO_2-rich

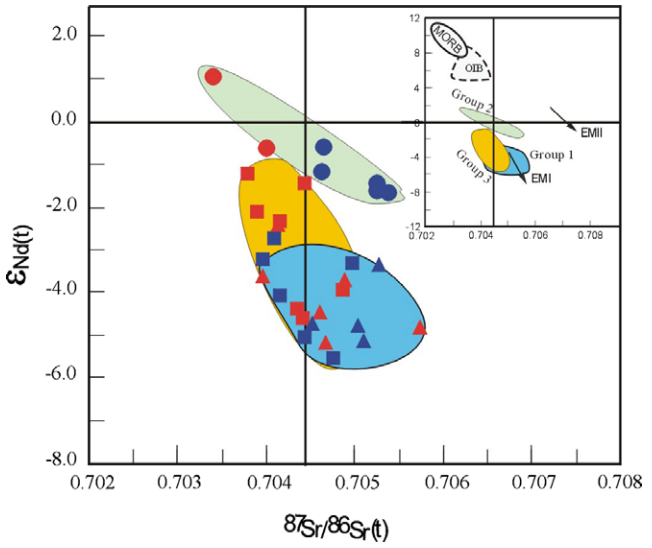

Fig. 6. $\varepsilon_{Nd}(t)$ versus $^{87}Sr/^{86}Sr(t)$ diagram for the ~1770 Ma mafic dikes in the Trans-North China Orogen. The fields for the MORB, OIB, EMI and EMII mantle sources are from Hawkesworth et al. (1984) and Hart (1988). Symbols are the same as those in Fig. 4a.

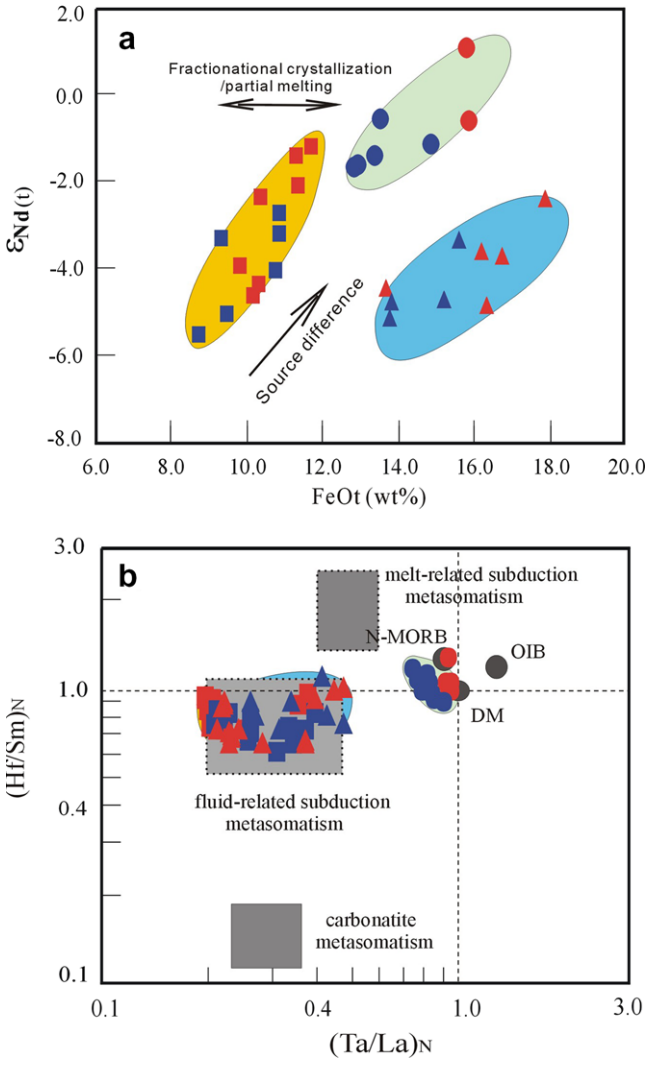

Fig. 7. Plots of FeOt versus $\varepsilon_{Nd}(t)$ (a), and $(Hf/Sm)_N$ versus $(Ta/La)_N$ (b) for the ~1770 Ma mafic dikes in the Trans-North China. The ranges of different sources in (b) are after Hofmann and Jochum (1996) and LaFlèche et al. (1998). Symbols are the same as those in Fig. 4a.

melt might result in an increasing orthopyroxene in the source due to the reaction of olivine with SiO_2 (metasomatic agent) (Chalot-Prat and Boullier, 1997), inconsistent with the preceding consideration. Therefore, the above-mentioned characteristics, including the depletion of Nb and Ta relative to LREEs, low $\varepsilon_{Nd}(t)$ values, and high LILEs/HREEs (/HFSEs) and $(Hf/Sm)_N$ ratios for Groups 1 and 3 rocks, more likely reflect the injection of subduction-related fluids into the mantle source. This is also supported by the trends shown in Figs. 8a and b. As a result, the petrogenesis of Groups 1 and 3 is more likely related to metasomatism of a lithospheric mantle by subduction-related fluids.

The most important difference between Groups 1 and 3 is that the former has higher FeOt contents (>12.5%) and the latter has a significant Th–U depletion relative to LREE (Figs. 3c and d). Although the petrogenesis of these high-Fe rocks is still enigmatic, three models can be used to explain the high-FeOt contents of Group 1 rocks: (1) the Fenner fractionation of primitive magma; (2) higher pressure or higher degrees of partial melting with respect to that of "normal" tholeiitic magma; and (3) inheritance of a mantle source. Ti/Ti* ratios, as a signature of oxidation state, range from 0.52 to 0.87 for Group 1, which is similar to that of Group 3 (0.42–0.77). This is contrary to the observation that high-FeOt melts generally evolve at a relatively lower oxidation state than "normal" tholeiitic magma (Juster and Grove, 1989). The negative correlations of SiO_2 with FeOt and MgO for Group 1 (within the range of 49–55% of SiO_2) suggest magma evolution towards a Si-rich and Fe-poor trend, which is contrary to that for the Fenner fractionation. Experimental results show that FeOt in melts is positively correlated to pressure and, at a given pressure, the FeOt, MgO and Al_2O_3 increase with increasing degrees of partial melting (Hirose and Kushiro, 1993; Klemme et al., 2002; Kogiso et al., 2003). However, Group 1 has lower Al_2O_3 and higher FeOt than "normal" tholeiitic magma at comparable MgO. It is common that Zr/Y and TiO_2/Al_2O_3 ratios increase with the increasing melting pressure or with the decrease of melting degree due to decrease of Al_2O_3 in clinopyroxene and the increasing stability of garnet in the residue with increasing pressure (e.g. Walter, 1998; Ichiyama et al., 2006). Group 1 with high-FeOt contents generally shows lower Zr/Y ratios than those with low FeOt contents at comparable TiO_2/Al_2O_3 ratios. Considering that almost all Group 1 rocks have (Gd/Yb)cn of <2.0, we infer that high-FeOt of Group 1 should not be directly related to the degree of partial melting and depth of melt segregation, and that garnet is not an important residual phase in the source. Accordingly, a more reasonable explanation is that the high-FeOt contents of Group 1 were inherited from a metasomatised source.

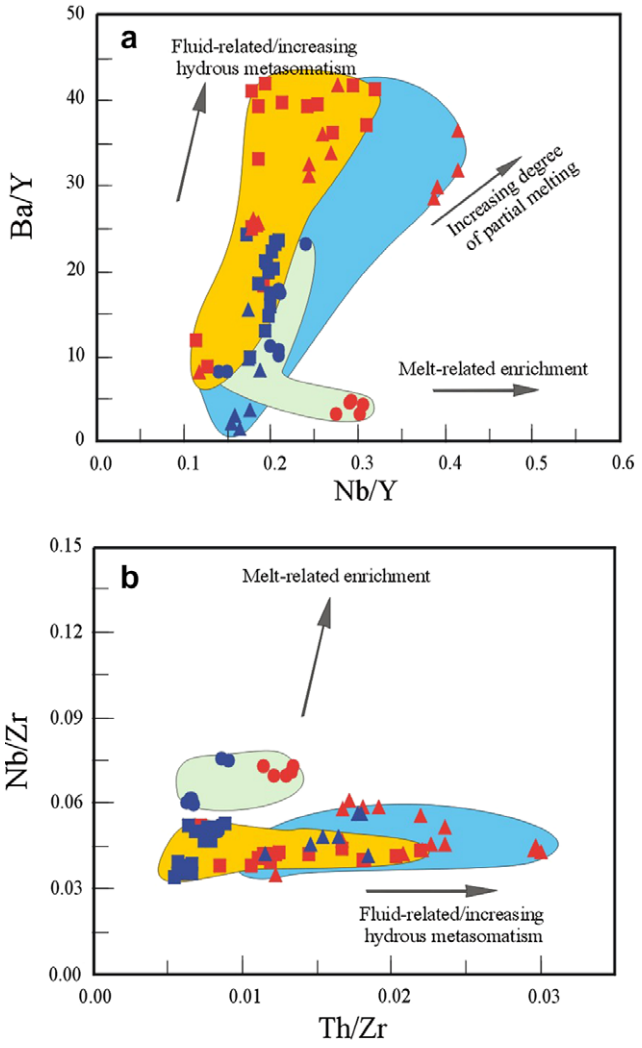

Fig. 8. (a) Ba/Y versus Nb/Y, (b) Nb/Zr versus Th/Zr, for the ~1770 Ma mafic dikes in the Trans-North China Orogen. The range and trend shown in (a–b) are from Hofmann and Jochum (1996), Kepezhinskas et al. (1997) and Sobolev et al. (2000), respectively. Symbols are the same as those in Fig. 4a.

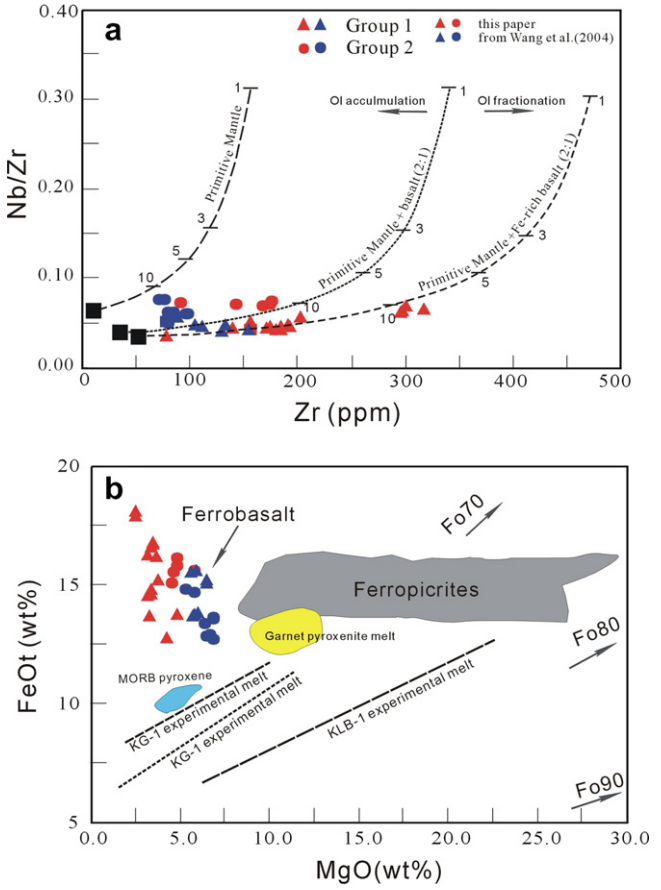

Fig. 9. (a) Nb/Zr versus Zr for the Group 1 and 2 mafic dikes. (b) The MgO–FeOt diagram of the Groups 1 and 2 mafic dikes. The calculated compositional paths of the batch melting of the primitive mantle, the peridotite + basalt (represented by eclogite) and the peridotite + Fe-rich basalt in (a) are from Ichiyama et al. (2006). Partition coefficients are after Halliday et al. (1995). The mineral proportion is olivine/orthopyroxene/clinopyroxene/garnet = 0.55:0.25:0.15:0.05 in primitive mantle and clinopyroxene/garnet = 0.5:0.5 in eclogite. The primitive mantle + basalt (eclogite) is a mixture of 2:1. The Zr and Nb contents of primitive mantle and eclogite (basalt) are 9.71 ppm, 0.6175 ppm and 104.24 ppm, 3.507 ppm, respectively (Hofmann, 1988). The composition of Fe-rich eclogite is represented by average composition of Fe-rich basaltic glasses with 208.8 ppm of Zr and 7.35 ppm of Nb (Regelous et al., 1999). The compositional melt of KLB-1 (anhydrous peridotite), KG-1 (peridotite/basalt = 2:1), KG-2 (peridotite/basalt = 2:1), MORB-like pyroxenite and garnet pyroxenite are from Hirose and Kushiro (1993), Kogiso et al. (2003), Hirschmann et al. (2003) and Pertermann and Hirschmann (2003). Also shown are ferropictites from Ichiyama et al. (2006). Symbols in (b) are the same as those in (a).

The question remains as to what kind of a mantle source possibly contains high-FeOt contents.

Mantle plume with Fe-rich eclogitic streaks (e.g. Herzberg and Zhang, 1996; Gibson et al., 2000; Kerrich et al., 1999) is a candidate for the source of high-FeOt melts because eclogitic streaks/blobs could be 50% partially melted at <3.0 GPa pressure to produce Al_2O_3- and FeOt-rich melt (Klemme et al., 2002; Rapp et al., 1991; Cordery et al., 1991; Gasparik and Litvin, 2002). However, all high-Fe rocks from a plume display OIB (or MORB)-like geochemical signatures, with positive $\varepsilon_{Nd}(t)$ values (up to +6) and high $(Nb/La)_N$ ratios (Gibson, 2002 and references therein). This is not the case for Group 1 rocks. An alternative way of generating the high-FeOt magma with the subduction-related signatures is by partial melting of a metasomatised mantle with eclogitic/pyroxenitic blobs/pods (e.g. Hauri, 1996; Takahasi et al., 1998; Leybourne et al., 1999), similar to a "re-fertilized" mantle source with recycled basaltic components (Yaxley and Green, 1998; Gasparik and Litvin, 2002). In Fig. 9a, Group 1 plot along the calculated compositional path of peridotite + Fe-rich basalt-derived melts (Ichiyama et al., 2006), suggesting that a basaltic component is more likely involved in the magma source of Group 1. The results of melting experiments show that a ferrobasalt (like Group 1, Fig. 9b) could have originated from a mantle source with low Fo values, such as a peridotite + basalt (pyroxenite) source (Kogiso et al., 2003; Hirose and Kushiro, 1993; Hirschmann et al., 2003; Pertermann and Hirschmann, 2003).

Melting experiments also reveal a peridotite source with basalt/veined pyroxenite as another possible candidate for producing a ferrobasalt with high Al_2O_3 contents (Kogiso et al., 2003; Pertermann and Hirschmann, 2003; Hirschmann et al., 2003). Thus, a "re-fertilized" peridotite source might give high-Fe contents (Gibson, 2002 and references therein), and the preferred partial melting will further increase FeOt and Al_2O_3 contents in the melt due to the moderately incompatible affinity of FeOt and Al_2O_3 (Hirose and Kushiro, 1993; Yaxley and Green, 1998). As a result, a significant mafic component related to either a recycled oceanic crust or a recycled mafic component of the continental crust is required to be responsible for a "re-fertilized" peridotite source.

Usually, recycled oceanic crust has high Nb/La ratios and $\varepsilon_{Nd}(t)$ values (Hofmann and Jochum, 1996; Sobolev et al., 2000). The reaction between recycled oceanic crust and peridotite may produce silica-undersaturated garnet pyroxenite (Cooke and O'Brien, 2001; Melluso et al., 2005). Such signatures are distinct from those of Group 1 rocks. Alternatively, a recycled mafic component of the continental crust may explain the geochemical features of Group 1. In the Trans-North China Orogen, most mafic rocks in the Jiehekou/Jingangku Formations show $(Nb/La)_N = 0.35–0.65$ and $\varepsilon_{Nd}(t) = -2.1$ to -5.0 at 1750 Ma (Liu et al., 2003). Therefore, recycled crustal materials could possibly be carried into the mantle as eclogitic/pyroxenitic pods to hybridize mantle peridotites (Hemond et al., 1994).

As described above, Group 3 rocks have lower FeOt contents than Group 1 rocks. In the diagram (Fig. 10a) of $(Th/La)_N$ versus $(Th/Ba)_N$, Group 3 displays similar $(Th/La)_N$ but lower $(Th/Ba)_N$ ratios in comparison with those of the Hawaiian volcanoes (Sobolev et al., 2000). The Th–U depletion is very likely related to plagioclase accumulation since plagioclase has extremely low Th/Pb and U/Pb ratios (Gancarz and Wasserburg, 1977; Sobolev et al., 2000) and possesses low partition coefficients for Th and U relative to La (LaTourette et al., 1995). The involvement of a gabbroic component might explain such a feature because a small amount of plagioclase in the gabbroic rocks could significantly change the Th–U partition in the melts. Based on the modeling calculations and geochemical characteristics, Wang et al. (2004) suggested that the negative Th–U anomalies for Group 3 are related to the involvement of recycled continental plagioclase-rich gabbros. Oceanic gabbros are likely to have substantial positive Sr and smaller positive Eu anomalies (Hofmann and Jochum, 1996; Sobolev et al., 2000) and they are distinct from the characteristics of Group 3 rocks. Therefore, a metasomatised lithospheric mantle with a minor continental gabbroic crustal component is proposed for the petrogenesis of Group 3.

5.3.2. Group 2

The mildly enriched geochemical characteristics of Group 2 mafic dikes are revealed by flat REE and slightly

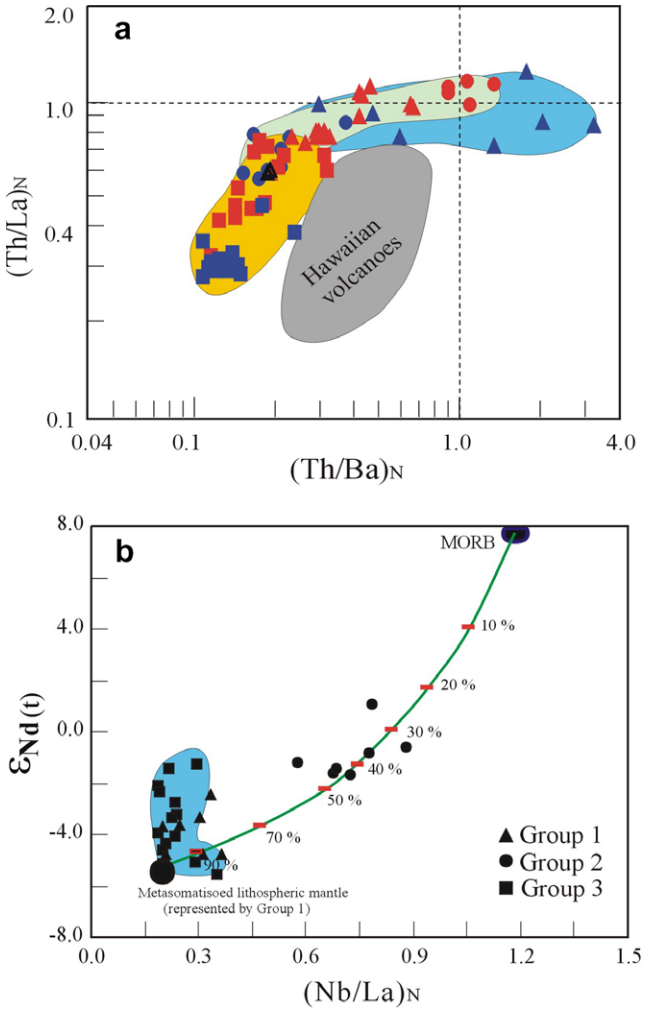

Fig. 10. Plots of (a) $(Th/Ba)_N$ versus $(Th/La)_N$, and (b) $(Nb/La)_N$ versus $\varepsilon_{Nd}(t)$ for the ~1770 Ma mafic dikes in the Trans-North China Orogen. The range shown in (a) is from Sobolev et al. (2000). Symbols in (a) are the same as those in Fig. 4a.

declining primitive-mantle normalized incompatible elemental patterns, as well as near-zero $\varepsilon_{Nd}(t)$ values. Almost all these rocks have Zr/Nb ratios between 13.6 and 14.7, lower than that of normal MORB (>17). The ratios of incompatible elements (e.g. La/Nb, Ba/Nb and Th/La, Ta/La and Hf/Sm) of Group 2 are different from those of a typical OIB or MORB (Table 1). Low (Gd/Yb)cn (<1.5) and (La/Yb)cn (<2.8) ratios indicate that the magma was produced by partial melting at shallow depth where garnet was not a residual phase in the source at the time of melt separation (Melluso et al., 2005; Storey et al., 1999). The relatively high contents of FeOt (>12.5 wt%) and TiO_2 (up to 2.67 wt%) are different from those of "normal" basaltic melts derived from a MORB-like source. It is obvious that these geochemical characteristics are not easily reconciled with shallow melting of suboceanic mantle. Similar to that of Group 1, a basaltic or Fe-rich basaltic component is required to explain the petrogenesis of Group 2 (Figs. 9a and b). Therefore, we propose that the parental magma was likely derived from

a MORB source contaminated by an Fe-rich lithospheric component, which appears to be the typical composition of Group 1 rocks.

Assuming that a Fe-rich metasomatised lithospheric component had Nd = 7 ppm, $(Nb/La)_N = 0.20$ and $\varepsilon_{Nd}(t) = -5$, and a MORB component had Nd = 2 ppm, $(Nb/La)_N = 1.2$ and $\varepsilon_{Nd}(t) = +8$ (Taylor and McLennan, 1985; Hawkesworth et al., 1984; Wang et al., 2004), a modeling calculation shows that addition of ~30% to 50% FeOt-rich component can produce the same observed variations in isotopic and incompatible elemental ratios (Fig. 10b). The participation of such a high proportion of FeOt-rich component would cause an increase in FeOt and Al_2O_3 contents of a hybridized source. Therefore, it is inferred that Group 2 was derived from a mixture of ~60% MORB and ~40% FeOt-rich metasomatised lithospheric mantle.

5.4. Tectonic implications

Two models have been proposed for the generation of the mafic dikes in the Trans-North China Orogen, one involves a mantle plume related to the break-up and dispersal of the North China Craton from other cratons (Zhao et al., 2002a,b; Zhai and Liu, 2003; Peng, 2005) and the second involves a post-collisional extensional event in response to the upwelling of convective mantle (Zhao et al., 2005; Wang et al., 2004). Our data provide important constraints to this debate. Group 1 mafic dikes were probably derived from a metasomatised lithospheric mantle with a recycled continental basaltic component, like a "re-fertilized" peridotitic source. Group 2 was originated from a mixture of a metasomatised Fe-rich lithospheric mantle with a MORB component. Group 3 was the product of a subduction-modified lithospheric mantle hybridized by a gabbroic component. Such a petrogenetic model for the ~1770 Ma mafic dikes in the Trans-North China Orogen suggests that the sources of these dikes were related to subduction–collision processes during or prior to the magma generation.

All studied samples show arc-like elemental and isotopic signatures. This is inconsistent with a plume-related origin for the dike magmas as it would they would be characterized by OIB-like elemental and isotopic compositions. Equally, Group 1 magma with high-FeOt contents could not be interpreted as the product of high-pressure melting of mantle plume with eclogitic streaks as discussed above. Moreover, a plume-derived Fe-rich melt is commonly regarded as the product of a plume starting-head and occurs only at the base of continental flood basalt provinces (Gibson et al., 2000; Hanski and Smolkin, 1995; Wooden et al., 1993). Besides, the melt is often followed by voluminous "normal" tholeiitic magma. However, such large amount of volcanic rocks is not found in the Trans-North China Orogen. These dikes in the Trans-North China Orogen were crystallized at ~1770 Ma, younger than that of the Paleoproterozoic crustal thickening and uplifting of the Orogen (~1870 to 1790 Ma; Wang et al., 2003; Zhao et al., 2005 and references therein), and also earlier than the age of crystallization of the unmetamorphosed mafic dikes in the Eastern Block (~1840 Ma; Hou et al., 2006; Wang et al., 2007). Such an observation is inconsistent with regional-scale upwelling of a major plume associated with the dikes.

Based on the above discussion, we infer that the Archaean Eastern and Western Blocks developed independently during the Archaean time, and collided along the Trans-North China Orogen at ~1.85 Ga and the dikes were emplaced in a post-collisional extensional regime (e.g. Wang et al., 2003, 2004). The source regions of Paleoproterozoic mafic dikes in the Trans-North China Orogen had been modified by the subduction/collision shortly after the amalgamation of the two Blocks. The FeOt-rich magma has commonly higher density than "normal" magma, thus the transport of FeOt-rich magmas to the surface/subsurface requires rapid rifting or a divergent tectonic regime (Brooks et al., 1991). Thus, the occurrence of Groups 1 and 2 FeOt-rich magmas is consistent with a rifting regime. We propose that such a post-collisional extension regime led to partial melting of a subduction-modified lithospheric mantle mixed with the basaltic/gabbroic rocks, and generation of Groups 1 and 3 magmas with high-FeOt and island-arc geochemical affinity. The interaction of convective mantle with the subduction-modified mantle results into generation of Group 2 magma.

Acknowledgements

The authors would like to thank M. Sun, M.G. Zhai and W.L. Xu for their thorough, critical and constructive reviews and comments, and B.-M. Jahn and K. Burke for their helpful editorial advise. We would like to thank Dr. J.-F. Ying for helpful discussions and suggestions, and Drs. X.-Y. Chen and J.-W. Zhi for assistance in preparing samples. Financial support is jointly provided by Chinese Academy Sciences (KZCX2-yw-128), Hong Kong RGC Projects (HKU7055/03P, 7048/03P, 7058/04P and 7055P) and the Natural Science Foundation of China (40334039 and 40473019). This is Tectonics Special Research Centre Publication No. 414 and is a contribution to International Lithosphere Program ERAS (EaRth Accretionary Systems in space and time).

References

Brooks, C.K., Larsen, L.M., Nielsen, T.F.D., 1991. Importance of iron-rich tholeiitic magmas at divergent plate margins: a reappraisel. Geology 19, 269–272.

Cawood, P., Wilde, S.A., Wang, K.Y., Nemchin, A., 1998. Integrated geochronology and field constraints on subdivision of the Precambrian in China: data from the Wutaishan. Abstract of the 9th International Conference on Geochronology, Cosmochronology and Isotope Geology, Beijing. Chinese Science Bulltin, vol. 43, p. 17.

Chalot-Prat, F., Boullier, A.M., 1997. Metasomatism in the subcontinental mantle beneath the Eastern Carpathians (Romania): new evidence

from trace element geochemistry. Contrib. Miner. Petrol. 129 (4), 284–307.

Cooke, R.A., O'Brien, P.J., 2001. Resolving the relationship between high P–T rocks and gneisses in collisional terrane: an example from the Gföhl gneiss-granulite association in the Moldanubian Zone, Austria. Lithos 58, 33–54.

Cordery, M.J., Davies, G.F., Campbell, I.H., 1991. Genesis of flood basalts from eclogite-bearing mantle plumes. J. Geophys. Res. 102, 20179–20197.

Gancarz, A.J., Wasserburg, G.J., 1977. Initial Pb of the Amitsoq genesis. West Greenland and implications for the age of the Earth. Geochim. Cosmochim. Acta 41, 1283–1301.

Gao, S., Zhang, B.R., Jin, Z.M., Kern, H., Luo, T.C., Zhao, Z.D., 1998. How mafic is the lower continental crust? Earth Planet. Sci. Lett. 161 (1–4), 101–117.

Gasparik, T., Litvin, Y.A., 2002. Experimental investigation of the effect of metasomatism by carbonatic melt on the composition and structure of the deep mantle. Lithos 60 (3–4), 129–143.

Gibson, S.A., 2002. Major element heterogeneity in Archean to recent mantle plume starting-heads. Earth Planet. Sci. Lett. 195, 59–74.

Gibson, S.A., Thompson, R.N., Dickin, A.P., 2000. Ferropicrites: geochemical evidence for Fe-rich streaks in upwelling mantle plumes. Earth Planet. Sci. Lett. 174, 355–374.

Halliday, A.N., Lee, D.C., Tommasini, S., Davies, G.R., Paslick, C.R., Fitton, J.G., James, D.E., 1995. Incompatible trace elements in OIB and MORB and source enrichment in the sub-oceanic mantle. Earth Planet. Sci. Lett. 133, 379–395.

Halls, H.C., Li, J.H., Davis, D., Hou, G.T., 2000. A precisely dating Proterozoic palaeomagnetic pole from the North China craton and its relevance to palaeocontinental reconstruction. Geophys. J. Int. 143, 185–203.

Hammouda, T., 2003. High-pressure melting of carbonated eclogite and experimental constraints on carbon recycling and storage in the mantle. Earth Planet. Sci. Lett. 214 (1–2), 357–368.

Hanski, E.J., Smolkin, V.F., 1995. Iron- and LREE-enriched mantle source for early Proterozoic intraplate magmatism as exemplified by the Pechenga ferropicrites. Kola Peninsula Russia. Lithos 34, 107–125.

Hart, S.R., 1988. Heterogeneous mantle domains: signature, genesis and mixing chronologies. Earth Planet. Sci. Lett. 90, 273–296.

Hauri, E.H., 1996. Major-element variability in the Hawaiian mantle plume. Nature 382, 415–419.

Hawkesworth, C.J., Rogers, N.W., van Calsteren, P.W.C., Menzies, M.A., 1984. Mantle enrichment processes. Nature 311 (27), 331–335.

HBBGMR (Bureau of Geology and Mineral Resources of Hebei Province), 1989. Regional geology of Beijing, Tianjin and Heibei Province. Geology Public House, Beijing, pp. 50–241 (in Chinese).

Hemond, C., Devey, C.W., Chauvel, C., 1994. Source compositions and melting processes in the Society and Austral plumes (South Pacific Ocean): element and isotope (Sr, Nd, Pb, Th) geochemistry. Chem. Geol. 115, 7–45.

Herzberg, C., Zhang, J.Z., 1996. Melting experiments on anhydrous peridotite KLB-1: compositions of magmas in the upper mantle and transition zone. J. Geophys. Res. 101, 8271–8295.

Hirose, K., Kushiro, I., 1993. Partial melting of dry peridotites at high pressures: determination of compositions of melts segregated from peridotite using aggregates of diamond. Earth Planet. Sci. Lett. 114, 477–489.

Hirschmann, M.M., Kogiso, T., Baker, M.B., Stolper, E.M., 2003. Alkalic magmas generated by partial melting of garnet pyroxenite. Geology 31, 481–484.

Hofmann, A.W., 1988. Chemical differentiation of the Earth: the relationship between mantle, continental crust, and oceanic crust. Earth Planet. Sci. Lett. 90, 297–314.

Hofmann, A.W., Jochum, K.P., 1996. Source characteristics derived from very incompatible trace elements in Mauna Loa and Mauna Kea basalts, Hawaii Scientific Drilling Project. J. Geophys. Res. 101 (B5), 11831–11839.

Hou, G.T., Liu, Y.L., Li, J.H., 2006. Evidence for ~1.8 Ga extension of the Eastern Block of the North China Craton from SHRIMP U–Pb dating of mafic dike swarms in Shandong Province. J. Asian Earth Sci. 27 (4), 392–401.

Ichiyama, Y., Ishiwatari, A., Hirahara, Y., Shuto, K., 2006. Geochemical and isotopic constraints on the genesis of the Permian ferropicritic rocks from the Mino–Tamba belt, SW Japan. Lithos 89 (1–2), 47–65.

IMBGMR (Bureau of Geology and Mineral Resources of Inner Mongolia Autonomous Region), 1991. Regional Geology of Inner Mongolia Autonomous Region. Geol Pub House, Beijing 1991, 1–725p (in Chinese).

Jensen, L.S., 1976. A new cation plot for classifying subalkaline volcanic rocks. Ontario Geology Survey, Miscellaneous, p. 66.

Juster, T.C., Grove, T.L., 1989. Experimental constraints on the generation of Fe-Ti basalts, andesites and rhyodacites at the Galapagos Spreading Center, 85°W and 95°W. J. Geophys. Res. 94 (B7), 9251–9274.

Kepezhinskas, P., McDermott, F., Defant, M.J., Hochstaedter, A., Drummond, M.S., 1997. Trace element and Sr–Nd–Pb isotopic constraints on a three-component model of Kamchatka Arc petrogenesis. Geochim. Cosmochim. Acta 61 (3), 577–600.

Kerrich, R., Polat, A., Wyman, D., Hollings, P., 1999. Trace element systematics of Mg- to Fe-tholeiitic basalt suites of the superior province: implications for Archean mantle reservoirs and greenstone belt genesis. Lithos 46, 163–187.

Klemme, S., Blundy, J.D., Wood, B.J., 2002. Experimental constraints on major and trace element partitioning during partial melting of eclogite. Geochim. Cosmochim. Acta 66 (17), 3109–3123.

Kogarko, L.N., Kurat, G., Ntaflos, T., 2001. Carbonate metasomatism of the oceanic mantle beneath Fernando de Noronha Island, Brazil. Contrib. Miner. Petrol. 140 (5), 577–587.

Kogiso, T., Hirschmann, M.M., Frost, D.J., 2003. High-pressure partial melting of garnet pyroxenite: possible mafic lithologies in the source of ocean island basalts. Earth Planet. Sci. Lett. 16 (4), 603–617.

Kröner, A., Wilde, S.A., Zhao, G.C., O'Brien, P.J., Sun, M., Liu, D.Y., Wan, Y.S., Liu, S.W., Guo, J.H., 2006. Zircon geochronology and metamorphic evolution of mafic dikes in the Hengshan Complex of northern China: evidence for late Palaeoproterozoic extension and subsequent high-pressure metamorphism in the North China Craton. Precambrian Res. 146 (1–2), 45–67.

Kröner, A., Wilde, S.A., Li, J.H., Wang, K.Y., 2005. Age and evolution of a late Archaean to early North China Craton. Precam. Res. 146(1–2), 45–67. Paleozoic upper to lower crustal section in the Wutaishan/Hengshan/Fuping terrain of northern China. J. Asian Earth Sci. 24 (5), 577–595.

Kusky, T.M., Li, J.H., 2003. Paleoproterozoic tectonic evolution of the North China Craton. J. Asian Earth Sci. 22, 383–397.

LaFlèche, M.R., Camiré, G., Jenner, G.A., 1998. Geochemistry of post-Acadian, Carboniferous continental intraplate basalts from the Maritimes basin, Magdalen islands, Québec, Canada. Chem. Geol. 148, 115–136.

LaTourette, T., Hervig, R.L., Holloway, J.R., 1995. Trace element partitioning between amphibole, phlogopite and basanite melt. Earth Planet. Sci. Lett. 135, 13–30.

LeBas, M.J., LeMaitre, R.W., Streckeisen, A., Zanettin, B., 1986. A chemical classification of volcanic rocks based on the total alkali-SiO_2 diagram. J. Petrol. 27, 745–750.

Leybourne, M., Wangoner, N.V., Ayres, L., 1999. Partial melting of a refractory subducted slab in a paleoproterozoic island arc: implications for global chemical cycles. Geology 27 (8), 731–734.

Li, J.H., Kröner, A., Qian, X.L., O'Brien, P., 2000. Tectonic evolution of an early precambrian high-pressure Granulite belt in the North China Craton. Acta Geol. Sinica 74, 246–258.

Liang, X.R., Wei, G.J., Li, X.H., Liu, Y., 2003. Precise measurement of $^{143}Nd/^{144}Nd$ and Sm/Nd ratios using multiple-collectors inductively couple plasma-mass spectrometer (MC–ICP-MS). Geochimica 32 (1), 91–96.

Liu, J.Z., Zhang, F.Q., Ouyang, Z.Y., Li, C.L., Zhou, Y.L., Xu, L., 2003. Geochemistry and chronology of the Jiehekou Group metamorphic

basic volcanic rocks in the Lüliang Mountain area, Shanxi, China. Sci. China (Ser. D) 46 (11), 1171–1181.

Liu, Y., Liu, H.C., Li, X.H., 1996. Simultaneous and precise determination of 40 trace elements in rock samples using ICP-MS. Geochimica 25 (6), 552–558.

Melluso, L., Morra, V., Brotzu, P., Tommasini, S., Renna, M.R., Duncan, R.A., Franciosi, L., D'Amelio, F., 2005. Geochronology and petrogenesis of the cretaceous Antampombato–Ambatovy complex and associated dike swarm, Madagascar. J. Petrol. 46 (10), 1963–1996.

Peng, P., 2005. Petrogenesis and tectonic significance of the about 1.8 Ga mafic dike swarms in the Central North China Craton. Ph.D. Thesis. Institute of Geology and Geophysics, CAS, Beijing.

Peng, P., Zhai, M.-G., Zhang, H.-F., Zhao, T.P., Ni, Z.-Y., 2004. Geochemistry and geological significance of the 1.8 Ga mafic dike swarms in the North China craton: an example from the juncture of Shanxi, Hebei, and Inner Mongolia: Acta Petrol. Sinica. 20 (3), 439–456 (in Chinese with English abstract).

Pertermann, M., Hirschmann, M.M., 2003. Anhydrous partial melting experiments on MORB-like eclogite: phase relations, phase compositions and mineral/melt partitioning of major elements at 2–3 GPa. J. Petrol. 44, 2173–2201.

Rapp, R.P., Watson, E.B., Miller, C.F., 1991. Partial melting of amphibolite eclogite and the origin of Archean trondhjemites and tonalites. Precambrian Res. 51 (1–4), 1–25.

Regelous, M., Niu, Y., Wendt, J.I., Batiza, R., Greig, A., Collerson, K.D., 1999. Variations in the geochemistry of magmatism on the East Pacific Rise at 10830VN since 800 ka. Earth Planet. Sci. Lett. 168, 45–63.

Rudnick, R.L., Fountain, D.M., 1995. Nature and composition of the continent-crust: a lower crustal perspective. Rev. Geophys. 33 (3), 267–309.

Sobolev, A.V., Hofmann, A.W., Nikogosian, I.K., 2000. Recycled oceanic crust observed in 'ghost plagioclase' within the source of Mauna Loa Lavas. Nature 404 (27), 986–990.

Storey, B.C., Leat, P.T., Weaver, S.D., Pankhurst, R.J., Bradshaw, J.D., Kelley, S., 1999. Mantle plumes and Antarctica–New Zealand rifting: evidence from mid-Cretaceous mafic dikes. J. Geol. Soc. 156, 659–671.

Sun, S.S., Mcdonough, W.F., 1989. Chemical and isotopic systematic of ocean basalt: implications for mantle composition and processes. In: Saunders, A.D., Norry, M.J. (Eds.), Magmatism in the Ocean Basin, vol. 2. Geol Soc Spec Pub, pp. 313–345.

SXBGMR (Bureau of Geology and Mineral Resources of Shanxi Province), 1989. Regional geology of Shanxi Province. Geol Pub House, Beijing, pp. 1–780 (in Chinese).

Takahasi, E., Nakajima, K., Wright, T.L., 1998. Origin of the Columbia River basalts: melting model of a heterogeneous plume head. Earth Planet. Sci. Lett. 162, 63–80.

Taylor, S.R., McLennan, S.M., 1985. The Continental Crust: Its Composition and Evolution. Blackwell, Oxford Press, pp. 1–312.

Walter, M.J., 1998. Melting of garnet peridotite and the origin of komatiite and depleted lithosphere. J. Petrol. 39, 29–60.

Wang, Y.J., Fan, W.M., Zhang, Y.H., 2004. Geochemical, $^{40}Ar/^{39}Ar$ geochronological and Sr–Nd isotopic constraints on the origin of Paleoproterozoic mafic dikes from the southern Taihang Mountains and implications for the 1800 Ma event of the North China Craton. Precambrian Res. 135 (1–2), 55–79.

Wang, Y.J., Fan, W.M., Zhang, Y.H., Guo, F., 2003. Structural evolution and $^{40}Ar/^{39}Ar$ dating of the Zanhuang metamorphic domain in North China Craton: constraints on Paleoproterozoic tectonothermal overprinting. Precambrian Res. 122 (1–4), 159–182.

Wang, Y.J., Zhao, G.C., Fan, W.M., Peng, T.P., Sun, L.H., Xia, X.P., 2007. LA–ICP-MS U–Pb zircon geochronology and geochemistry of Paleoproterozoic mafic dikes from western Shandong Province: Implications for back-arc basin magmatism in the Eastern North China Craton. Precambrian Res. 154 (1–2), 107–124.

Winchester, J.A., Floyd, P.A., 1977. Geochemical discrimination of different magma series and their differentiation products using immobile elements. Chem. Geol. 20, 325–343.

Wooden, J.L., Czamanske, G.K., Fedorenko, V.A., Arndt, N.T., Chauvel, C., Bouse, R.M., King, B.S.W., Knight, R.J., Siems, D.F., 1993. Isotopic and trace-element constraints on mantle and crustal contributions to Siberian continental flood basalts, Noril'sk area, Siberia. Geochim. Cosmochim. Acta 57, 3677–3704.

Yaxley, G.M., Green, D.H., 1998. Reactions between eclogite and peridotite: mantle refertilisation by subduction of oceanic crust. Schweiz. Miner. Petrogr. Mitt. 78, 243–255.

Yaxley, G.M., Green, D.H., Kamenetsky, V., 1998. Carbonatite metasomatism in the southeastern Australian lithosphere. J. Petrol. 39 (11–12), 1917–1930.

Zhai, M.G., Liu, W.J., 2003. Paleoproterozoic tectonic history of the North China Craton: a review. Precambrian Res. 122, 183–199.

Zhang, B.R., Luo, T.C., Gao, S., Ouyang, J.P., Chen, D.X., Ma, Z.D., 1994. Geochemical Study of the Lithosphere, Tectonism and Metallogenesis in the Qinling-Dabashan Region. Press of China University Of Geosciences, Wuhan, pp. 1–446.

Zhao, G.C., Cawood, P.A., Wilde, S.A., Sun, M., Lu, L., 2000. Metamorphism of basement rocks in the central zone of the North China Craton: implications for Paleoproterozoic tectonic evolution. Precambrian Res. 103, 55–88.

Zhao, G.C., Sun, M., Wilde, S.A., Li, S.Z., 2003. Assembly, accretion and breakup of the Paleo-Mesoproterozoic Columbia Supercontinent: records in the North China Craton. Gondwana Res. 6, 417–434.

Zhao, G.C., Sun, M., Wilde, S.A., Li, S.Z., 2005. Late Archean to Paleoproterozoic evolution of the North China Craton: key issues revisited. Precambrian Res. 136, 177–202.

Zhao, G.C., Wilde, S.A., Cawood, P.A., Sun, M., 2002a. SHRIMP U–Pb zircon ages of the Fuping complex: implications for late Archean to Paleoproterozoic accretion and assembly of the North China Craton. Am. J. Sci. 302, 191–226.

Zhao, T.P., Zhou, M.F., Zhai, M.G., Xia, B., 2002b. Paleoproterozoic rift-related volcanism of the Xiong'er Group, North China Craton: implications for the breakup of Columbia. Int. Geol. Rev. 44 (4), 336–351.